M.Tech. (Power Systems)

Md. Khalid Akhlaque

CONTROL ALGORITHMS MODELLING AND ANALYSIS FOR GRID-INTEGRATED SOLAR PV SYSTEM

A DISSERTATION

SUBMITTED IN PARTIAL FULFILLMENT FOR THE REQUIREMENTS OF THE AWARD OF THE DEGREE OF

MASTER OF TECHNOLOGY

IN

POWER SYSTEMS

SUBMITTED BY

MD. KHALID AKHLAQUE

(2K21/PSY/08)

UNDER THE SUPERSVISION OF

PROF. J. N. RAI

AND

PROF. S.T. NAGARAJAN

DEPARTMENT OF ELECTRICAL ENGINEERING

DELHI TECHNOLOGICAL UNIVERSITY

(Formerly Delhi College of Engineering)

Bawana Road, Delhi-110042

MAY, 2023

DEPARTMENT OF ELECTRICAL ENGINEERING

DELHI TECHNOLOGICAL UNIVERSITY

(Formerly Delhi College of Engineering)

Bawana Road, Delhi-110042

CANDIDATE'S DECLARATION

I, **Md. Khalid Akhlaque**, Roll No. **2K21/PSY/08**, of M.Tech. Power Systems, hereby declare that the project Dissertation titled "**CONTROL ALGORITHMS MODELLING AND ANALYSIS FOR GRID-INTEGRATED SOLAR PV SYSTEM**" which is submitted by me to the Department of Electrical Engineering, Delhi Technological University, Delhi in partial fulfilment of the requirement for the award of the degree of Master of Technology, is original and not copied from any source without proper citation. This work has not previously formed the basis for the award of any Degree, Diploma Associateship, Fellowship or other similar title or recognition.

Place: New Delhi

Date:

MD. KHALID AKHLAQUE

(2K21/PSY/08)

DEPARTMENT OF ELECTRICAL ENGINEERING

DELHI TECHNOLOGICAL UNIVERSITY

(Formerly Delhi College of Engineering)

Bawana Road, Delhi-110042

CERTIFICATE

We hereby, certify that the Project Dissertation titled "**CONTROL ALGORITHMS MODELLING AND ANALYSIS FOR GRID-INTEGRATED SOLAR PV SYSTEM**," submitted by **Md. Khalid Akhlaque**, Roll No. **2K21/PSY/08**, from the Department of Electrical Engineering, Delhi Technological University, Delhi, for the partial fulfilment of the requirements for the degree of Master of Technology, is an authentic record of the project work conducted by the student under our supervision. To the best of our knowledge, this work has not been submitted, either partially or in its entirety, for any degree or diploma at this University or any other institution.

Place: New Delhi

Date:

Prof. J. N. Rai
(SUPERVISOR)
DEPARTMENT OF
ELECTRICAL ENGINEERING
DELHI TECHNOLOGICAL
UNIVERSITY
New Delhi-110042

Prof. S. T. Nagarajan
(CO-SUPERVISOR)
DEPARTMENT OF
ELECTRICAL ENGINEERING
DELHI TECHNOLOGICAL
UNIVERSITY
New Delhi-110042

ACKNOWLEDGEMENT

I would like to express my deepest gratitude and appreciation to all those who have supported and contributed to the completion of this thesis.

First and foremost, I am indebted to my supervisors, **Prof J. N. Rai** and **Prof. S. T. Nagarajan**, for their invaluable guidance, unwavering support, and expert advice throughout this research journey. Their profound knowledge, insightful feedback, and constant encouragement have been instrumental in shaping the direction and quality of this thesis. I am truly grateful for their mentorship.

I am grateful to **Prof. Pragati Kumar**, Head of Department, Electrical Engineering, for providing me with consistent and continuous support for carrying out my research.

I would also like to express my sincere gratitude to **all the faculty members of the Department of Electrical Engineering,** for their time, expertise, and valuable input. Their constructive criticism and thoughtful suggestions have greatly enriched the content and clarity of this work.

Lastly, I would like to express my appreciation to my family and friends for their unwavering love, encouragement, and understanding throughout this challenging endeavour. Their belief in my abilities has been a constant source of motivation, and I am truly blessed to have them in my life.

PLACE: New Delhi
Date:

MD. KHALID AKHLAQUE
2K21/PSY/08
M.Tech (Power System)
DEPARTMENT OF
ELECTRICAL ENGINEERING
DELHI TECHNOLOGICAL
UNIVERSITY

ABSTRACT

In order to achieve sustainable growth, the integration of renewable energy sources, such as solar photovoltaic (PV) energy, with conventional energy sources is necessary. This requires advanced power systems equipped with modern theories and approaches. By integrating solar PV energy generation with the grid, the growing energy demand can be met while also acting as a stabilizing factor for the grid. This integration reduces the burden on the grid, minimizes losses through transmission and distribution lines, mitigates congestion, and enhances the overall grid's efficiency.

To ensure smooth integration, various components are employed, including the voltage source converter (VSC), which converts the DC power from the solar PV system into AC power for the grid. To prevent high-frequency switching ripples from being injected into the grid, filters are added at the output terminals of the VSC. Synchronization between the grid and VSC voltage in terms of frequency and phase angle is crucial. Loss of synchronization can have catastrophic effects on the entire grid system.

Another important aspect that needs attention is power quality (PQ). To mitigate PQ issues and avoid grid malfunctioning, several control algorithms have been developed. In this thesis, a novel Modified Versoria based Zero Attraction-LMS (MVZA-LMS) control algorithm is proposed. This algorithm incorporates a penalty factor based on the Versoria function into the basic Least Mean Square (LMS) algorithm to enhance its zero-attraction capability. The enhanced zero-attraction capability of the proposed algorithm improves convergence rate and modeling accuracy. The zero-attraction topology offers reduced computational complexity, easy implementation, and enhanced steady-state performance compared to other control algorithms. Examples of zero-attraction-based LMS techniques include the Robust ZA-LMS (RZA-LMS) technique, the polynomial zero-attraction (PZA)-LMS control algorithm, the l0-LMS technique, and the ZA-LMS technique.

The proposed control scheme focuses on maximizing power extraction from the PV array while addressing power quality concerns, including harmonics elimination, load balancing, and power factor improvement under time-varying scenarios. The MVZA-LMS algorithm enhances the dynamic performance, resulting in improved response

time and system robustness. This control scheme effectively addresses power quality issues and conditions the current by adjusting its weight component, especially when working with an underdeveloped grid that exhibits inferior power quality due to voltage distortions and imbalances. The performance of the proposed control scheme is compared with other zero attraction-LMS techniques, and MATLAB-Simulink is utilized for simulation and analysis. The proposed algorithm demonstrates improved efficacy in various situations, thereby increasing the efficiency of grid-tied solar PV systems

CONTENTS

List of Figures

List of Tables

List of Symbols

E: energy (joules)

h: Planck's constant (h = 6.63×10^{-34} joules-sec)

C: speed of light (2.988×108 m / s),

v: frequency of photons in Hz

λ: the wavelength of photons in meters, mostly expressed in μm

Energy is expressed in eV: electron volt (1 eV = 1.6×10^{-19} joules)

h_o overloading factor

m_{ind} modulation index

χ_{Pr} proportional

χ_{in} integral gain

ρ zero-attracting parameter

μ is the step size

η_b is efficiency of the boost converter

List of Abbreviations

I_{PHOTON}	Photocurrent of the Solar PV cell
R_S	Intrinsic series resistance
R_{SH}	Shunt resistance
SPV	Solar Photovoltaic
Solar PV	Solar Photovoltaic
INC	Incremental conductance
IR	Integral regulator
SPGS	Solar Power Generation System
ZA	Zero Attracting/Zero Attraction
P&O	Perturb and Observance
LMS	Least Mean Square
Is	Saturation Current
MVZA-LMS	Modified Versoria Zero Attracting Least Mean Square
RES	Renewable Energy Sources
RZA-LMS	Robust Zero Attracting Least Mean Square

CHAPTER 1

INTRODUCTION

1.1 Overview

"Energy is life", by saying this it can be inferred that for sustainable development and overall growth energy is prerequisite. Per capita energy consumption is the most important indicator for the growth of a country. Every country on this earth needs energy, especially electrical form of energy for their development. Energy can be classified into various forms but electrical energy is predominant, because of its easy handling, transportation, large scale generation, storing, controlling and translation into different forms. Developing nation are trying to catch the developed countries, leading to huge increase in electrical energy demand. Advancement in the power system technology and augmentation of new principles and theories has increased the generation capacity, but still there is a sharp gap between demand and supply.

Excessive exploitation of fossil fuels has been made to increase the generation, leading to environmental degradation and fossil fuels reserve's depletion. Scientist and engineers are very worried about the above-mentioned situations, and looking for renewable energy sources (RESs) as an alternative source of energy, which is inexhaustible and puts less or no impact on global environment to achieve sustainable growth. There are different types of RESs but we mostly talk of wind and Solar energy. The solar energy is growing has a great potential to replace conventional source of energy. Solar energy system can be used as standalone system and as a grid connected system. Grid-tied solar system plays a very crucial role in reducing burden, stabilizing and hence increases reliability, efficiency and performance of the grid. There are challenges and complexity while integrating Solar PV (SPV) system with grid and power quality issues arise. The various power quality issues and solutions has been discussed in later part of the thesis.

Table 1.1 Total installed capacity of India and its renewable energy share as on 30.04.2023 [58].

Power Sector at a Glance ALL INDIA

Updated on 15-05-2023		
1.Total Installed Capacity (As on 30.04.2023) **-** Source : Central Electricity Authority (CEA)		
INSTALLED GENERATION CAPACITY (SECTOR WISE) AS ON 30.04.2023		
Sector	**MW**	**% of Total**
Central Sector	1,00,055	24.0%
State Sector	1,05,726	25.4%
Private Sector	2,10,810	50.6%
Total	**4,16,591**	
Installed GENERATION CAPACITY(FUELWISE) AS ON 30.04.2023		
CATAGORY	**INSTALLED GENERATION CAPACITY(MW)**	**% of SHARE IN Total**
Fossil Fuel		
Coal	205,235	49.3%
Lignite	6,620	1.6%
Gas	24,824	6.0%
Diesel	589	0.1%
Total Fossil Fuel	**2,37,269**	**57.0 %**
Non-Fossil Fuel		
RES (Incl. Hydro)	**172,542**	41.4%
Hydro	**46,850**	**11.2 %**
Wind, Solar & Other RE	125,692	30.2 %
Wind	42,868	10.3 %
Solar	67,078	16.1 %
BM Power/Cogen	10,248	2.5 %
Waste to Energy	554	0.1 %
Small Hydro Power	4,944	1.2 %
Nuclear	6,780	1.6%
Total Non-Fossil Fuel	**179,322**	43.0%
Total Installed Capacity (Fossil Fuel & Non-Fossil Fuel)	**4,16,91**	**100%**

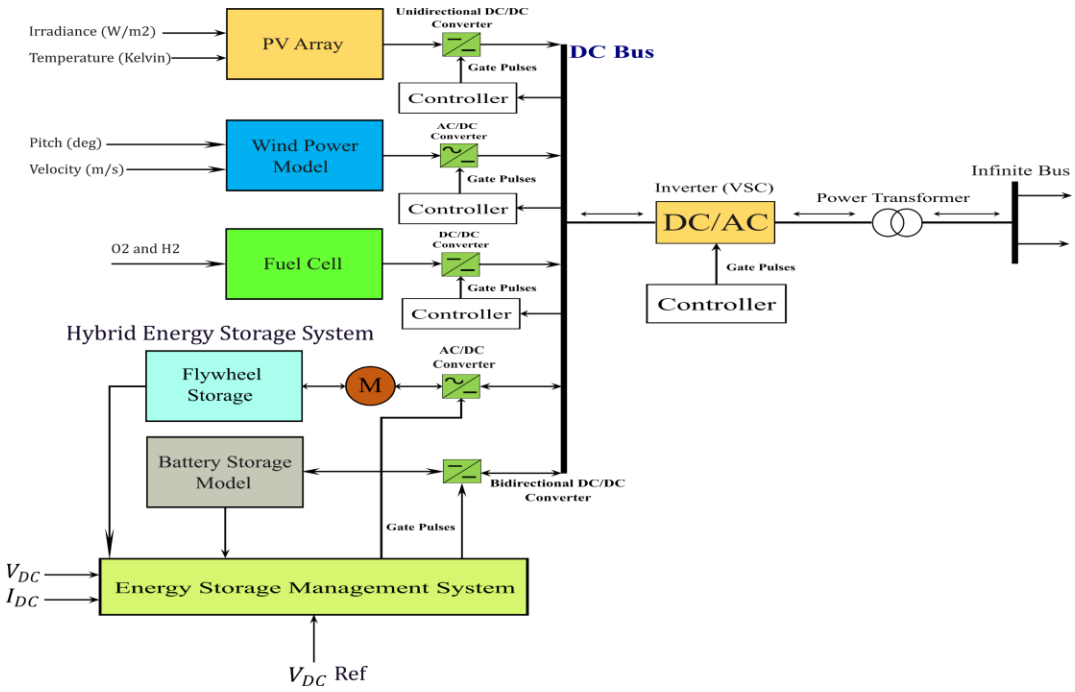

Fig. 1.1 Block diagram of RES

1.2 Modern Distribution System and Power Quality (PQ)

I t is desired from the modern distribution system to incorporate the rise in demand on time without compromising reliability, safety and cost effectiveness. It does not seem to be simple, because of its large size, complexity and at the same time huge energy loss and interruption occurs because of faults [30]. One more thing that is needed from Modern distribution system (MDS) is to ensure quality power to the loads. Good quality of power should also be maintained at generation, utilization and transmission level [31, 32]. The abnormality at the utilization end is quite severe. Plenty of reasons are there for abnormality in Ac supply system, Natural cause such as faults, flashover, lightening, equipment failure and induced or forced ones, which includes notches and voltage distortion are few of them. So many consumers' equipment also contributes in polluting the distribution system because it draws non-sinusoidal current and the load act as a non-linear load. As power quality is measured in deviation in frequency, current and voltage which may lead to maloperation or failure of the consumer's equipment. At the point of common coupling (PCC) where different loads are connected, some voltage base PQ problems present at that point are spikes, fluctuations, voltage harmonics, sag/dip, glitches, surge, swell, flickers, unbalance, notches and outages and many more. Various non-linear loads consist of adjustable speed drives (ASDs),

uninterruptible power supplies (UPSs), and furnaces and different types of disturbance are the main reasons for these problems in the distribution system. However, some current related PQ problems are harmonic currents, unbalanced currents, bad power factor, reactive power burden, and an excessive neutral current in polyphase systems because of generation of harmonic currents due to nonlinear loads and unbalancing.

These PQ problems cause capacitor banks failure, losses will be increased in the electric machines and distribution system, resonance causes excessive current and over voltages, motors and alternators experiences negative sequence currents, heating of rotor, breakdown of insulation, interfering in communication systems, false metering, malfunction in the operation of breaker and relay and many more. Different mitigation approach is employed for existing system and newly designed equipment because their power quality issues are different for the distribution systems and loads. Low pf, unbalanced currents, harmonic currents, and an excessive neutral current are the PQ issues pertaining to existing non-linear loads, can be fixed with help of series of filter such as passive, active and combination of both (hybrid) connected in a different fashion, which externally used based on the nature of load. In distribution system there might occur a PQ problem other than harmonics, power devices like unified power quality conditioners (UPQCs), distribution static compensators (DSTATCOMs), and dynamic voltage restorers (DVRs) are customised to mitigate voltage and current associated PQ issues [36-40].

1.3 State of the Art

Solar energy system can be utilized in two different mode, stand-alone system and grid-interfaced mode. Solar PV system has a non-linear characteristic due to dependency on solar irradiance and temperature, which is variable in nature, so there is a need for an algorithm to track the peak power point and extract maximum power out of SPV all the time. P&O, INC, ANN-based and Fuzzy-logic based are the few amongst many MPPT algorithm available with us. In this work, INC with integral regulator has been used.

Grid plays a very crucial role of transferring bulk power to fulfill the demand. Integrating SPV system with grid and transferring power, causes power quality (PQ) issues. Power quality control of a 3-phase grid-tied SPV system under different scenarios such as normal and abnormal conditions, connected to unbalanced loads have

been dealt and discussed at length through numerous Literature. This work encompasses the development of an algorithm to allay the issues pertaining to power quality and hence quality power can be ensured.

1.4 Scope of the work

After reviewing various literature on 3-phase grid-integrated SPV system, inference can be drawn that various control model such as Least Mean Fourth (LMF), Least Mean Square (LMS) and its variants, Adaline based Adaptive control algorithm, Power Balance Theory (PBT) and Fuzzy-Logic Based have been developed and used to improve the performance of voltage source converter (VSC). But still they not free from error, lot more work is needed to be done to improve the performance. For example, if we increase the step size of Least Mean Square (LMS) based VSC control algorithm, convergence rate will be high but steady-state oscillation will increase, which ultimately reduces the controller performance under various scenario. So, there is a need to create a perfect balance between these two aspects.

Precisely, objective of this proposed work is to design a control algorithm model for 3-phase grid-tied SPV system to mitigate issues pertaining to PQ. The proposed control methodology adjusts the weight component of the Load current. Zero steady-state error, reliable, robust, fast dynamic performance, and less complex are desirable features of the proposed algorithm. A performance comparison will also be made with other available control technique.

1.5 Outline of the Thesis

Chapter 1: The first chapter consists of introduction to RESs, power quality issues

Chapter 2: It consists of various literature reviews on SPV system, power quality MPPT technique, DC-boost converter, voltage source converter (VSC) and control algorithm technique.

Chapter 3: This chapter includes basics of SPV system, MPPT algorithm, DC-boost converter, calculating values of various component, VSC and Hysteresis Current Controller.

Chapter 4: This chapter includes various control algorithm and their mathematical modelling and unit template calculation.

Chapter 5: Simulation, Results and Analysis of the various control algorithms.

Chapter 6: It includes Conclusion and future work scope.

CHAPTER 2

LITERATURE REVIEW

2.1 Overview

Integration of SPV to the grid is done to increase the supply by injecting active power to it. To attract the maximum power from SPV, modelling with precision has to be studied and developed so that it matches practical SPV. Modern distribution system with variable loads which leads to power quality issues is reviewed. This chapter includes the review on various control techniques to make performance better and robust under varying load scenario. Detailed reviews on various system configuration have been discussed.

2.2 Literature Review on SPV Modelling

As per **[10][17]** a SPV cell is modelled on the basis of single and double diode insertion. Bellia et al [2014][15] talks about single-diode model based solar cell with shunt and series resistances reduces complexity while resembling with practical cell. Amorphous silicon based solar cell and multi junction production cell, whose efficiency may vary from less than 10% to more than 40% respectively when designed in a controlled environmental condition **[12,13][10].** Solar PV cell is not intermittent, highly dependent on environmental conditions such temperature, solar insolation, pollution etc. and hence reduces efficiency. In practice we can deduce only 15% to 22% from the cell **[14-15][10].** Solar PV cell based on current source and its characteristic is non-linear [10]. In [3-7][10] the need for grouping of cells in different fashion has been explained to achieve the desired power.

2. 3 Literature Review on MPPT Technique and Inverter

MPPT algorithm is required to fetch maximum power from SPV array. So many research work is available on MPPT algorithm [18-23]. In [18-20] perturb and observe (P&O) algorithm has been explained, and also suggested how simple and cost effective

this method is. P&O method is not free from drawback is [21]. INC MPPT technique is explained in [21-28]. INC MPPT algorithm has superior performance than P&O MPPT algorithm, but it has its own shortcomings [22-23]. An improved INC algorithm has been developed to overcome the problems of classical INC technique. INC with integral regulator (IR) has been explained in literature [26] in great detail. INC with IR MPPT algorithm eliminates the error present in classical INC and improves the performance of MPPT technique to locate the MPP very precisely and accurately [26-28]. In the proposed work INC with IR MPPT algorithm has been used. Literature [54-55] has discusses about VSC.

2.4 Literature Review on PQ issues

Modern day distribution system has become very large and its complexity increase with time. Quality power assurance is a big challenge for distribution systems. Distribution system incorporating new technologies to overcome these challenges [30]. As per [38] major losses occur near distribution end and that leads to a major power quality problem due to diversified loading conditions. Major PQ problems are short and long-time variations in voltage, flicker, waveform deformation and unbalanced voltage are few amongst many problems discussed in [38,39]. The reason behind these issues lightening stroke, flashover, non-linear loads, switching, various faults, power electronics devices like converters and arc furnaces. If power quality issue is not taken care off, it may lead to system's maloperation, failure of electrical equipment, large scale power loss which will disrupt the supply and huge financial loss will be done [57]. Extensive use of power electronics devices can cause harmonics in distribution at PCC, which is worrying the engineers and researchers. Communication channels can also be disturbed by harmonic currents present in the ac system due to non-linear load which alters the sinusoidal nature of AC. There might occur a resonance, while performing reactive power compensation for power factor correction, which is highly undesirable feature in power system. Institute of Electrical and Electronics Engineers (IEEE) has suggested and recommended Power quality standards [53] for engineers, practitioners and researchers.

Advancement in switching devices has increased the usage of STATCOM to allay the power quality problems as mentioned in [58]. Now a days Insulated Gate Bipolar Transistor (IGBT) is in high demand, which is robust and performs better switching as

compared to the earlier used Metal Oxide Semiconductor Field Effect Transistor (MOSFET) and Gate Turn Off Thyristor (GTO) [58]. Power filters in different arrangements like series, shunt or in hybrid model can be employed to overcome PQ issues [37-40]. The PQ issues pertaining to voltage like voltage fluctuation, flicker, surge, harmonics and unbalanced voltage can be eliminated by employing series active filter [38] [35, 36] [43]. The literature [35-38] discusses about DSTATCOM, which is a shunt active filter and can act as a VSC and Current Source Inverter (CSI) [37]. Current related problem like power factor improvement, voltage regulation, harmonics and load balancing can be eliminated by DSTATCOM.

2.5 Literature Review on VSC Control Algorithm

For sustainable development and growth of a country, integration of RESs with the existing grid is necessitated. Integration of RESs system can cause many power quality issues as listed in [38]. VSC is needed to convert DC power from SPV into AC to transmit to the grid [53,54]. To ensure the improvement in PQ, VSC must be controlled appropriately to mitigate the issues of PQ. Plenty of VSC control algorithm is available. Least Mean Square (LMS) algorithm estimates weight component of the load current and acts accordingly to control the VSC for desired output [51]. Chen et al [2016][44] explained that how it improves the convergence rate and performance of basic LMS technique by adding zero attracting component in the cost function of LMS to control VSC. In the literature [45][46][50], Zero attraction-LMS control algorithm has been designed for 3-phase grid-tied SPV system for power quality control. Robust Adaptive Algorithm (RZA-LMS) control algorithm is discussed in [56][52]. Bhattacharjee et al, [2020][47] discusses the Modified Versoria based Zero Attraction – LMS algorithm, which introduces the penalty factor based on Versoria function in the classical LMS algorithm to enhance zero attraction capability, ultimately increases the convergence rate and good modelling accuracy. Versoria based function mentioned in {48-49].

CHAPTER 3

VARIOUS COMPONENTS OF THE SOLAR POWER GRID SYSTEM

3.1 Photovoltaic System

Solar cells connected in series and parallel forms Solar PV module. The desired output can be achieved by using SPV Module. Solar Photovoltaic cell is nothing but a ***PN*** junction or simply a diode. Solar cell captures the sun light and directly transform it into electrical energy. Energy from the sun travels in the form of photons and is absorbed by semiconductors such as silicon or selenium. Energy higher than band gap energy of the semiconductor or equal is necessitated to excite the electron to move from low energy band level (valence band) to higher energy band level (conduction band) and ultimately lead to produce electron-hole pair. There is an inherent electric field which affects both the carriers in the depletion region and reduces the recombining potential of these carriers. Concentration of the carriers increases at junction as depletion region diffuse. Hence, voltage between external terminal of the junction is developed. The current generated because of photon will start flowing through this circuit if load is added between these terminals [10]. Number of electron-hole pair formed will determine the current in an external circuit. When illumination falls on SPV cell bulk of electron-hole pair developed across the material, hence current flows through an electrically-shorted PN junction. Photoconduction is highly dependent on illumination intensity, duration and wavelength. In the absence of light or with dwindled intensity, conductivity will be reduced.

The energy available in a photon is given by:

$$E = \frac{hv}{\lambda} = \frac{hC}{\lambda} \tag{3.1}$$

Where E is in joules h is Planck's constant (h = 6.63×10^{-34} joules-sec), C is the speed of light (3×10^{8} m / s), v is frequency of photons in Hz and λ is the wavelength of photons in meters. Expressing λ in μm and energy in eV (1 eV = 1.6×10^{-19} joules).

Single-diode model shown in Fig. 1 is used to avoid complexity [11]. Accuracy is also one of the fundamental features of the model, it cannot be compromised with simplicity, hence a good balance is chalked out between these two features so the model can be optimized. The current source and a diode in parallel are the components of the basic structure. For a solar PV cell shown in Fig. 3.1, photocurrent is represented by I_{ph} while internal series and shunt resistances are exhibited by R_S and R_{Sh} respectively.

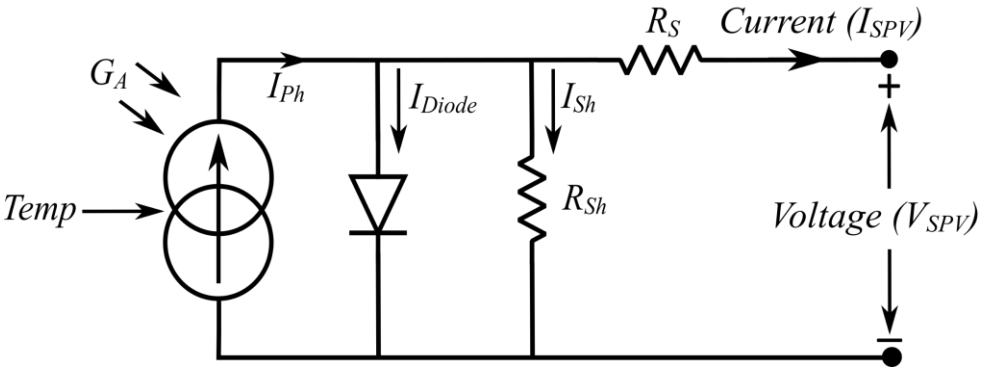

Fig. 3.1 Single diode PV cell

3.2 Mathematical Expression of Solar PV Module

Large number of SPV cells are combined together to form SPV module, and to design SPV array, modules are further grouped in series and parallel combination, so that the desired output power can be extracted from the PV system. Mathematical equation is given below which explain the I-V characteristics of the PV module [3-7].

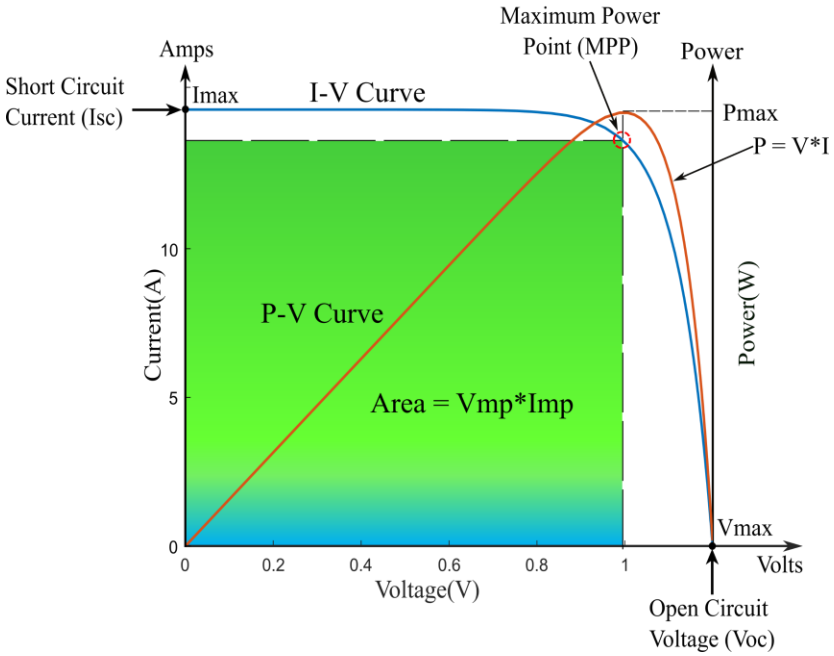

Fig.3.2 P-V and I-V Characteristics of SPV cell

3.2.1 Photocurrent (I_{Ph})

$$I_{Ph} = \left[I_{SCR} + K_I\left(T_A - T_{Ref}\right)\right] * \frac{G}{1000} \tag{3.2}$$

I_{Ph} (Amp) is generated current due to light at a given temp and solar irradiance (25°C and 1000 W/m^2). Short-circuit current/temperature coefficient is represented by K_I(0.0017A/K). Actual temperature is denoted by T_A and reference temperature by T_R in Kelvin. Solar insolation falls on solar cell surface is depicted by G in W/m^2. Short circuit current of the module is I_{SCR}.

3.2.2 Reverse Saturation Current I_{RS}

$$I_{RS} = \frac{I_{SCR}}{[\exp(QV_{OC}/n_{SL}\, k\alpha T_A) - 1]} \tag{3.3}$$

n_{SL} is number of series connected cell

k is Boltzmann constant whose value is 1.3805 × 10^{-23} J/K

α is the ideality factor

Q is charge (1.6 × 10^{-19} C)

V_{OC} open circuit voltage in Volt

3.2.3 Saturation Current (I_S)

$$I_S = I_{RS}\left[\frac{T_A}{T_{Ref}}\right]\exp\left[\frac{Q * E_{G0}}{\alpha * k}\left\{\frac{1}{T_{Ref}} - \frac{1}{T_A}\right\}\right] \quad (3.4)$$

E_{G0} is Band Energy Gap of semiconductor ($E_{G0} \approx 1.1$ eV for the polycrystalline Si at 25°C).

3.2.4 Output Current (I_{SPV})

$$I_{SPV} = n_{PL} * I_{Ph} - n_{PL} * I_S\left[\exp\left\{\frac{Q * (V_{SPV} + I_{PV}R_S)}{n_{SL}\alpha k T_A}\right\} - 1\right] - V_{SPV}\, I_{SPV} R_S / R_{Sh} \quad (3.5)$$

n_{PL} number of cells connected in parallel Equation (3.5) can be rewritten as

$$I_{SPV} = n_{SL} * I_{Ph} - n_{PL} * I_S\left[\exp\left\{\frac{Q * (V_{SPV} + I_{PV}R_S)}{n_{SL}\alpha k T_A}\right\} - 1\right] \quad (3.6)$$

Apollo Solar Energy ASEC-200G6S is used to design the SPV array, parameters of the module mentioned in the Table 3.1[2].

Table 3.1 Solar PV module and array parameters (Apollo Solar Energy ASEC-200G6S) at STC.

DESIGN OF SINGLE DIODE PV MODULE MODEL Apollo Solar Energy ASEC-200G6S	
PV MODULE	
SHORT CIRCUIT CURRENT (ISC)	8.24 A
OPEN CIRCUIT VOLTAGE (VOC)	33.53 V
VOLTAGE AT MPP, VMPP	25.38V
CURRENT AT MAXIMUM POWER POINT ,	7.89A
SOLAR PV ARRAY	
PV VOLTAGE AT MPP, VMPP	595 V
PV POWER AT MPP, PMPP	44 kW
PV CURRENT AT MPP, IMPP=PMPP/VMPP	IMPP=44000/(.8*700) = 78.6A
NUMBER OF SERIES MODULES n_{SL}	22 MODULES
NUMBER OF PARALLEL MODULES NP	10 MODULES

The SPV is dependent on environmental conditions such as solar irradiance and temperature. Current and voltage output of the Solar PV array will vary as according to the variation in environmental conditions such as temperature and solar insolation and hence, variation in P-V and I-V characteristics takes place. P-V and I-V curve of the

sample model is presented in Fig. 3.3. While considering all other parameters as constant, if the temperature increases, voltage will be reduced and hence, a loss of power will take place. On the contrary, if we reduce the temperature from a reference point, the increased output voltage and power will be harnessed from the cell. Fig. 3.3(a) shows that when temperature is increasing, on the X- axis voltage reduces. It can be deduced from the P-V curve of fig. 3.3(a) that if there is an increment in temperature, the power output will decrease. If we want to squeeze excess of energy from module, no other way but to enhance efficiency of the module. After going through various literatures [2-5] it can be inferred that while keeping all the parameters constant, if solar insolation is higher, current will increase an ultimately increased power will be produced. Fig. 3.3(b) simply validates our statements.

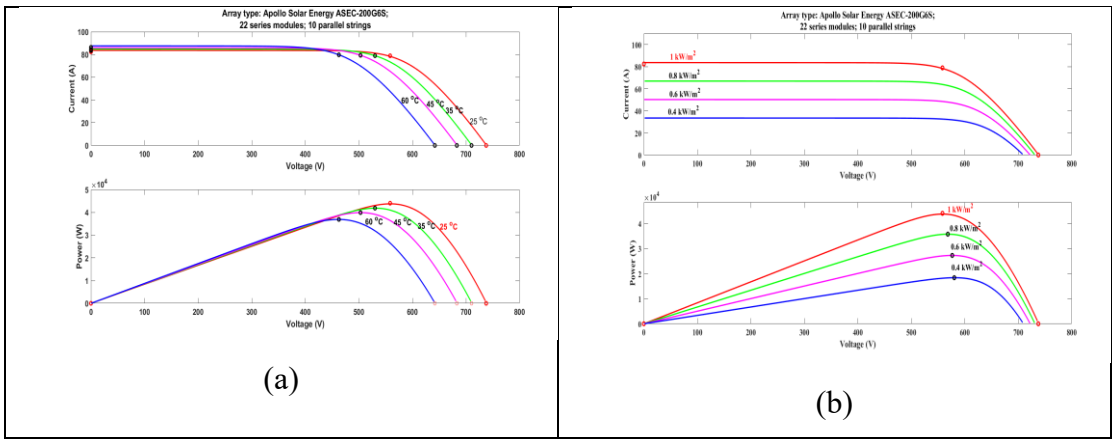

Fig 3.3. (a) P-V and I-V curve of a sample module at 1000 W/m^2 and for a given temperature. (b) P-V and I-V curve of a sample module at 25°C for a given insolation.

3.3 Maximum Power Point Tracking (MPPT) for Solar PV System

After analyzing SPV cell it has been concluded that the PV curve characteristic is non-linear and maximum power can be extracted from the cell at a specific point provided solar irradiance and temperature. MPPT technique is employed to track MPP and provide appropriate gating pulses to trigger the DC-DC boost converter which ensures the operation of PV module at maximum power point (MPP) always. Perturbation and Observation (P&O) and Incremental Conductance method (INC) are the few among several MPPT algorithms [18-20][29]. With the help of a block diagram MPPT control system is shown in Fig 3.4.

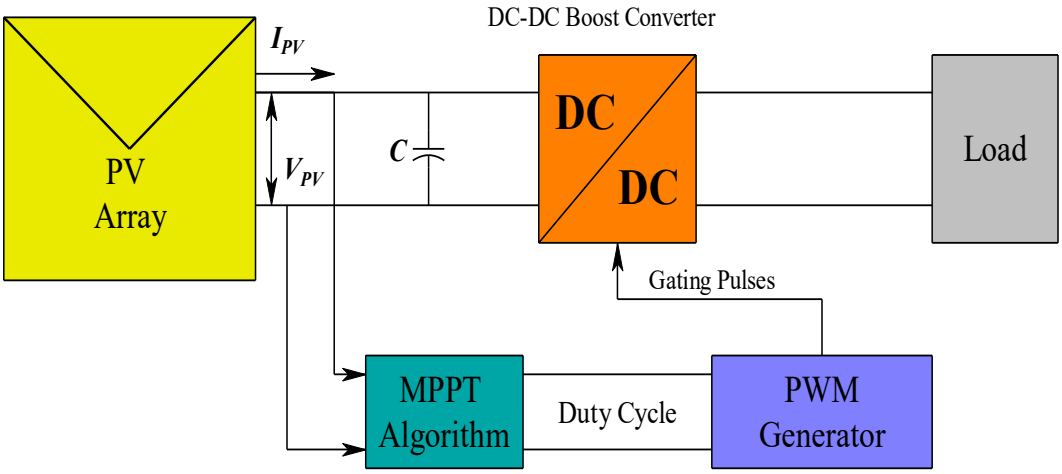

Fig 3.4 Block Diagram of MPPT Control System

3.3.1 Perturbation and Observation Methodology

Simple characteristics, low cost, and easy implementation are the major features of P&O MPPT methodology. Because of these features, P&O technique is very widely used and endorsed [18].

To ensure the point of operation at MPP, instantaneous power $P_{PV}(x)$ and voltage $V_{PV}(x)$ is measured by the system and then power difference and the voltage difference is recorded. The logic of P&O technique is explained below. It can be summarised in two cases [19].

Case I: if $\Delta P_{PV} > 0$, there arise two situations, as manifested in fig 3.5 (a) the operating point A and B. if $\Delta V_{PV} > 0$ then duty cycle for operating point A must be reduced to travel towards MPP and increase the duty ratio if $\Delta V_{PV} < 0$ for operating point B.

Case II: if $\Delta P_{PV} < 0$ two situation occurs, as displayed in fig 3.5(b), C and D points. For $\Delta V_{PV} < 0$, duty cycle must be decreased for operating point C and if $\Delta V_{PV} > 0$ increase the duty cycle for point D to travel towards MPP.

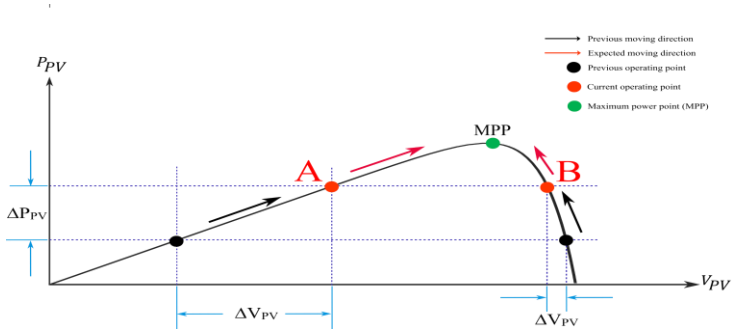

(a)

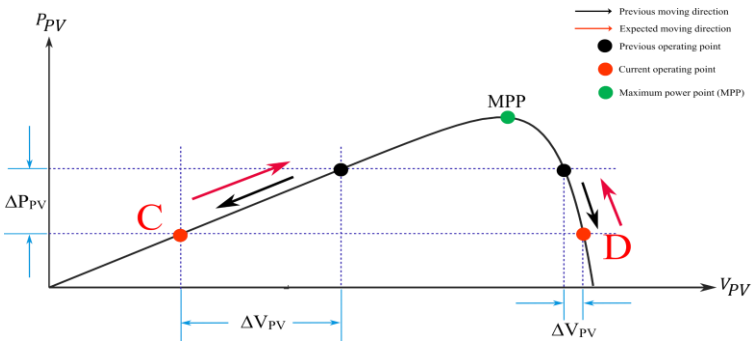

(b)

Fig. 3.5 (a) Positive power difference condition; (b) negative power difference condition [19].

Though P&O is the simplest technique and cost effective, but it is also not free from shortcomings such as tracking-speed and tracking-efficiency which invariably depends on step size of perturbation. If we made the step size small tracking will be slow but there will be minimal oscillation but transient response will be compromised, on the other hand if step size is increased, fast transient response is obtained but large steady-state oscillation will persist. Because of huge invariability in the environment, there is a need for fast response to locate MPP, so a judicious compromise has to be made between the above two responses, which ultimately decreases output power of the SPV array.

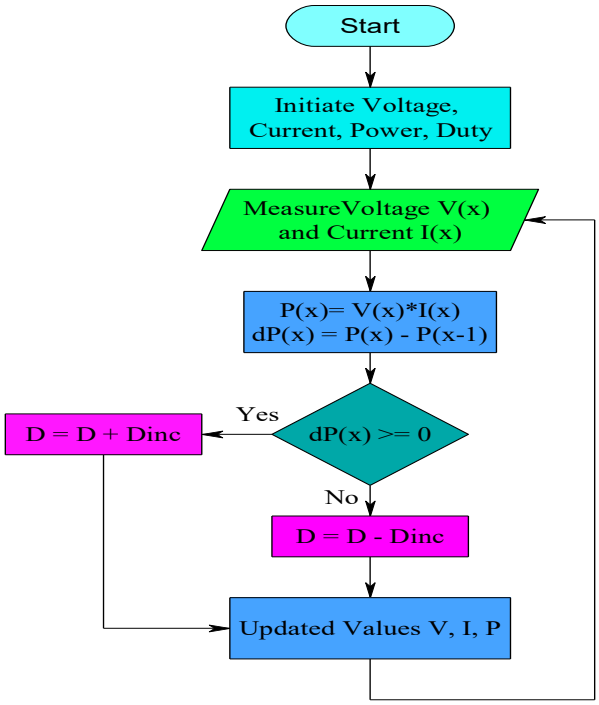

Fig 3.6 P&O Flow Chart [20]

3.3.2 Incremental Conductance Technique (INCT)

Incremental Conductance Technique (INCT) is used to overcome drawbacks pertaining to P&O. As per different literature [21, 22], P-V curve of the Solar PV(SPV) array can be divided into three region and accordingly the following equations can be deduced [23].

$$\text{At MPP,} \qquad dP_{PV}/dV_{PV} = 0 \tag{3.7}$$

$$\text{Left to MPP,} \quad dP_{PV}/dV_{PV} > 0 \tag{3.8}$$

$$\text{Right to MPP,} \quad dP_{PV}/dV_{PV} < 0 \tag{3.9}$$

so,

$$\frac{dV_{PV}}{dP_{PV}} = = d(I_{PV}V_{PV})/dV_{PV} = I_{PV} + V_{PV} * \left(\frac{dI_{PV}}{dV_{PV}}\right) \tag{3.10}$$

Equation (3.11) can be approximated as:

$$\frac{dV_{PV}}{dP_{PV}} \approx I_{PV} + V_{PV} * \left(\frac{\Delta I_{PV}}{\Delta V_{PV}}\right) \tag{3.11}$$

From equation (3.10) and (3.11) inference can be draw and the above equations (3.7, 3.8 and 3.9) is written as,

$$\text{At MPP,} \quad \frac{\Delta I_{PV}}{\Delta V_{PV}} = -\frac{I_{PV}}{V_{PV}} \tag{3.12}$$

$$\text{Left to MPP,} \quad \frac{\Delta I_{PV}}{\Delta V_{PV}} > -\frac{I_{PV}}{V_{PV}} \tag{3.13}$$

$$\text{Right to MPP,} \quad \frac{\Delta I_{PV}}{\Delta V_{PV}} < -\frac{I_{PV}}{V_{PV}} \tag{3.14}$$

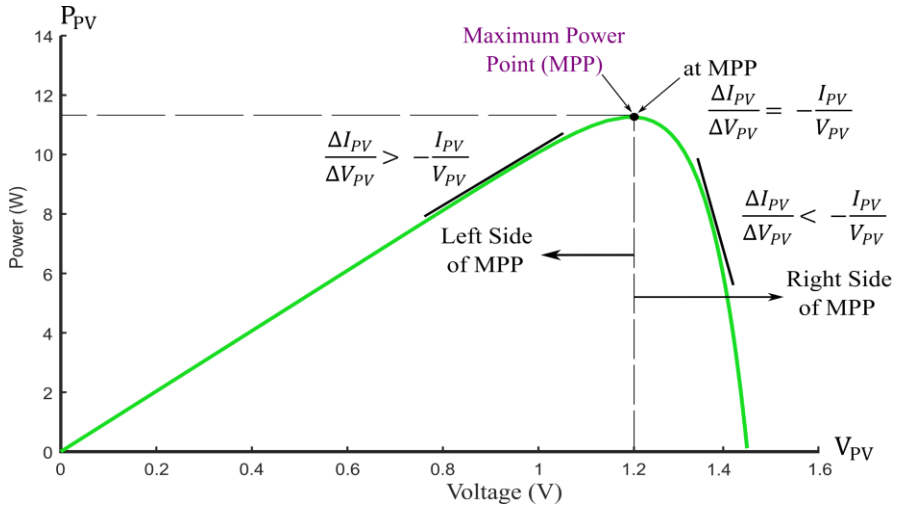

(a)

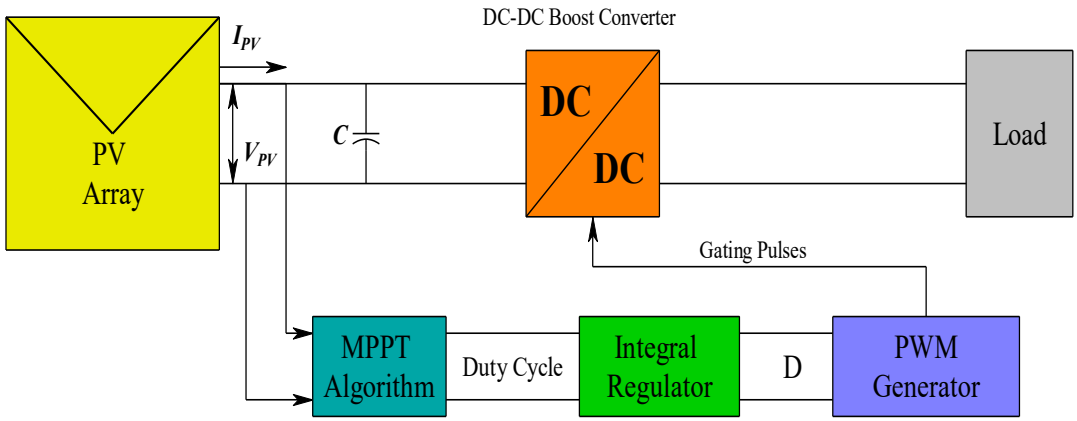

(b)

Swiftness of the MPP tracking will depend on step size, if it is large, faster will be the tracking. But there is a high chance that it will not be able to properly locate the MPP, but to oscillate near the MPP. Therefore, corrective measure has to be taken to improve

the control algorithm's performance. A strategic control instrument is implemented, where load resistance matches with the ratio of open circuit voltage to short circuit current ($\frac{V_{OC}}{I_{SC}}$) of SPV system. Even after having a good performance over P&O methodology under variable environmental circumstances, it can produce oscillations because of error signal induced in between the incremental and instantaneous conductance [26-27]

3.3.3 Integral Regulator Logic is used to Enhanced Incremental Conductance Performance.

INC technique can be understood by the equations (3.7 to 3.14). To eliminate the oscillations by reducing or mitigating error, improved efficacy and swift operation in locating MPP is done by incorporating integral regulator with basic INC as illustrated in Fig. 3.7 [28].

As per flow chart illustrated in fig. 3.7(c), small change in voltage pertains to slow controller feedback, leads to reduced output power. On the contrary if change in voltage is big, large oscillations occur due to compromised output. Error signal (e) puts a check on the oscillation's amplitude near MPP. If error is hight, amplitude of oscillation will be low. Moderate error value will cause the operating point to go away from the original MPP. So, great emphasis has to be given on choosing the error value with precision, to achieve the optimized performance of the controller. SPV array power will be consistent at MPP because of the adjustment made in the INC to make error zero. By introducing IR control logic, error because of instantaneous and incremental conductance can be eliminated [26]. Better operability, reduction in output oscillation, improved resolution and enhanced adaptability of the SPV system can be achieved by incorporating IR with INC algorithm, ultimately efficiency will be increased.

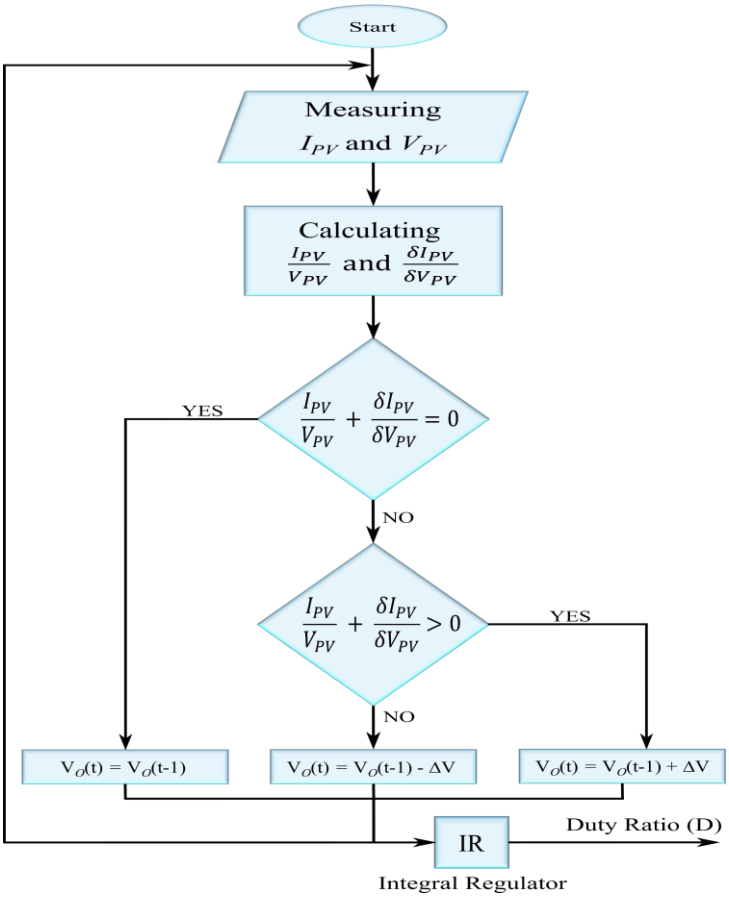

(c)

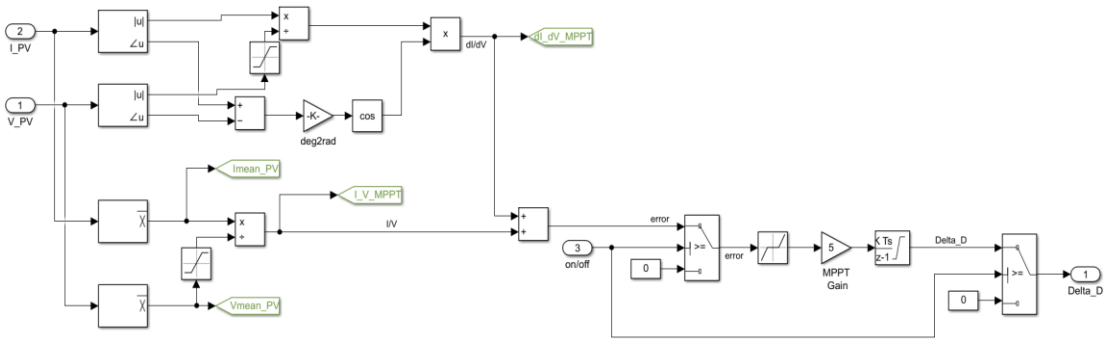

(d)

Fig 3.7 (a) PV module power curve (b) Block diagram of INC with Integral Regulator (IR) (c) Flow Chart of INC with IR [24] (d) Block diagram of Matlab Simulink INC MPPT with Integral Regulator Algorithm.

3.4 DC-DC Converter

The boost converter is employed to extract maximum power from SPV module. Basically, this converter steps up from low-level to high-level voltage. While designing MPPT controller DC-DC boost converter is incorporated [21, 22]. The circuit diagram of the boost converter is shown in fig.3.8. Various components of the converter are DC Voltage source (V_{IN}), load resistance, R_{LOAD}, DC filter capacitor (C_{DC}), Switch (S) boost inductor (L_{BOOST}), Diode and output DC voltage (V_{OUT}) [33-34].

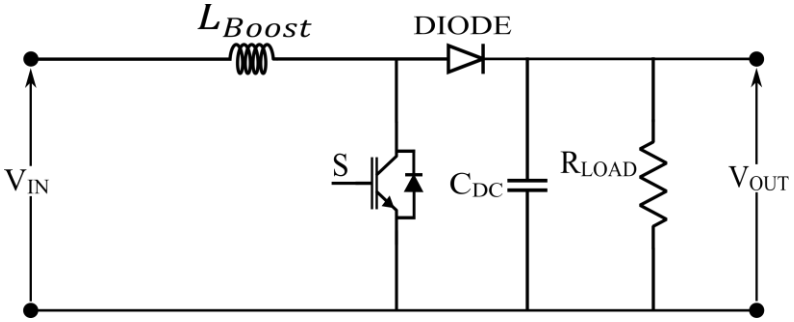

Fig. 3.8 Circuit diagram of DC-DC Boost Converter

3.4.1 Mathematical Calculation

$$M_{Gain} = \frac{V_{OUT}}{V_{IN}} = \frac{1}{1 - Duty\ Ratio} \tag{3.15}$$

From Eqn. (3.15) we can deduce, Duty Ratio (D)

$$Duty\ Ratio = 1 - \frac{V_{IN}}{V_{OUT}} * \eta_b \tag{3.16}$$

η_b is efficiency of the boost converter.

Value of inductor has to be designed in way that it should be greater than L_{MIN} always, which facilitates the continuous current operation of DC-DC boost converter. Hence,

$$L_{b0} = \frac{(1 - Duty\ Ratio^2) * Duty\ Ratio * R}{2f_{SW}} \tag{3.17}$$

f_{SW} is switching frequency. Alternatively, yielding capacitance with reference to output ripple voltage can be expressed as in equation (3.18)

$$C_{b0} = \frac{Duty\ Ratio}{R_{Load}(\Delta V_{OUT}/V_{OUT})\ f_{SW}} \tag{3.18}$$

3.5 Voltage Source Converter (VSC)

The Voltage Source Converter (VSC) has become a critical component finding its employment in the vast array of power electronic systems, like motor drives, power factor correction equipment, and the integration of renewable energy sources into the grid, among others. The Voltage Source Inverter (VSI), offers the highest level of efficiency, robustness, and faster dynamic response. Two-level VSCs are mostly utilized in low voltage, low power scenarios, with a minimal application in medium voltage systems [54, 55].

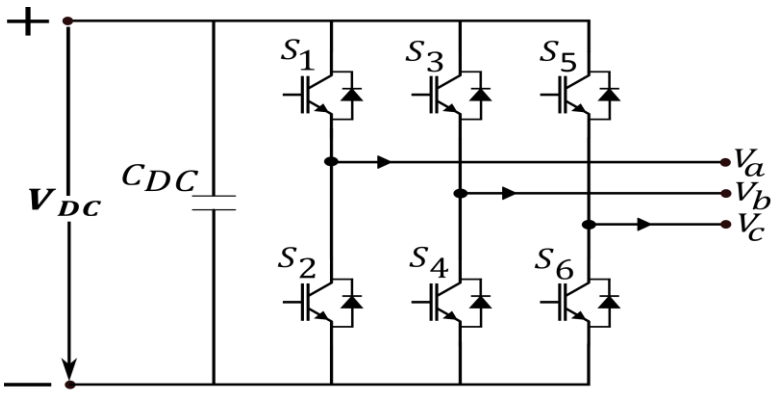

Fig. 3.9 IGBT based 3-phase, 2-Level Inverter Circuit

3.6 Current Controller

Pulse Width Modulation (PWM) technique is used to control the VSC by injecting gating pulses into. Hysteresis current controller (HCC) is a PWM controller, which is very common and popular due to its ease of deployment. HCC does not require any prior knowledge of the system parameter, and at the same time its response to the current loop is swift along with the ability to limit the inherent peak current. Switching condition to control VSC has been explained below.

If $I_L < (I_L^* - HB)$ upper and lower switch will OFF and ON respectively

If $I_L > (I_L^* + HB)$ upper and lower switch will ON and OFF respectively

Where I_L^* and I_L are reference and filter current respectively and Hysteresis band width is denoted by HB.

3.7 Solar PV System Design

Various components together form an SPGS, which is depicted in Fig.3.9 a two-stage, 44-kilowatt, 3-phase, SPGS tied with grid. SPV array, DC to DC converter with integral regulator INC MPPT. Capacitances, R-filters, various inductances, and inverter are the various components through which the system has been designed as per [45]. In order to transfer power to the grid, SPV unit is connected with the VSC at DC-link.

3.7.1 Solar PV Array Classification

The SPV array is further elaborated in [2], providing specific details. In this simulation, a three-phase, 50Hz, 415V grid is connected to the SPV array, which has a maximum power generation capacity of 44 kW. The subsequent subsection elucidates the formalization of estimating various components within the proposed model.

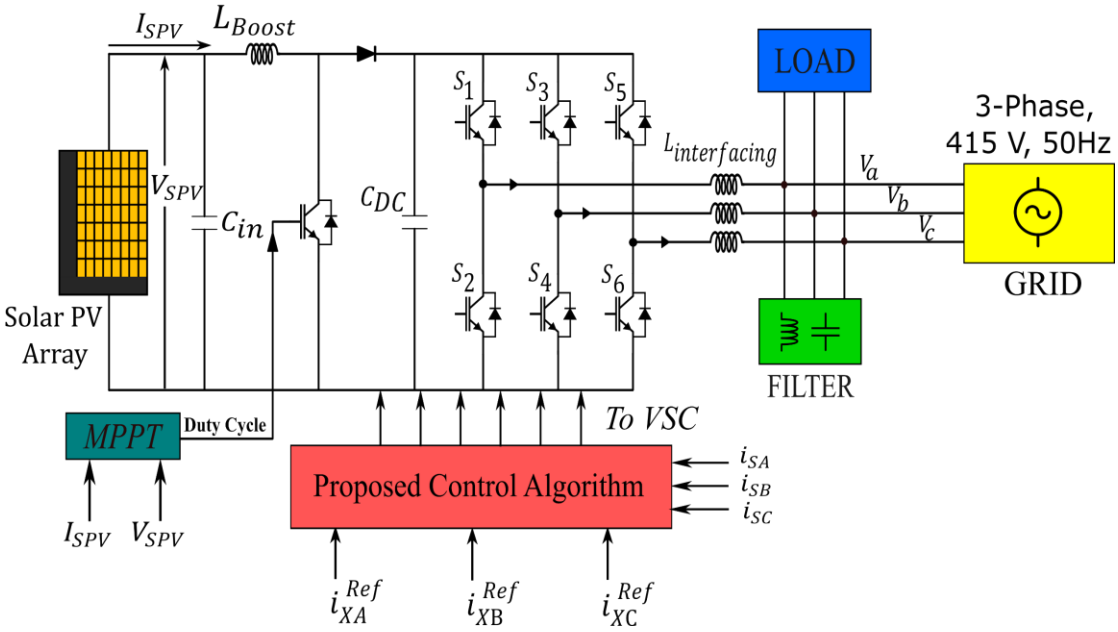

Fig 3.10 Circuit Diagram of a SPGS system

3.7.2 Designing DC-DC Boost Converter

Calculating inductor (L_{Boost}) value through equation (3.19) [45].

$$L_{Boost} = (V_M * D)/(\Delta I_l * f_{SW}) \tag{3.19}$$

The value of L_{Boost} is approximated as 3 mH.

V_M represents maximum power point voltage

f_{SW} is known as switching frequency

D stands for duty cycle

ΔI_l exhibits ripple in Solar PV

3.7.3 Selecting Voltage of DC-link

Equation (3.20) evaluates the value of the DC-link [45].

$$V_{DC} = 1.63 * \left(\frac{V_{LL}}{m_{ind}}\right) = 1.63 * \left(\frac{415}{1}\right) \approx 700 \quad (3.20)$$

m_{ind} is a modulation index. The value of m_{ind} is taken as 1, V_{LL} represents grid line voltage. V_{DC} is approximated as 700 V.

3.7.4 Selecting Interfacing Inductances

With the help of equation (3.21) Interfacing Inductances values can be calculated [45].

$$L_{IX} = \frac{m_{ind} * V_{DC}}{4 * h_o * f_{SW} * \Delta i_{RX}} \quad (3.21)$$

Wherein f_{SW} symbolizes the switching frequency, Δi_{RX} expresses the rated ripple current, m_{ind} exhibits the modulation index and h_o indicates the overloading factor. The L_{IX} value is set at 2.5 mH in this case.

3.7.5 Designing R-Filter

10 microfarads and 5 ohms, respectively, are selected as the filter's capacitance and resistance values [45].

3.5.6 Determination of DC-Link Capacitances

Using equation (3.22) the DC-link capacitances (C_{DC}) is computed [38].

$$C_{DC} = \frac{P_{DC}}{2 \times \omega * V_{DC} * (V_{DC-Ripple})} \quad (3.22)$$

wherein $V_{DC-Ripple}$ is the ripple voltage percentage. The approximated C_{DC} value is *6000 μF.* As a result, it can swiftly recalibrate the VSC DC link voltage during disturbances

CHAPTER 4

CONTROL ALGORITHM AND ITS MATHEMATICAL MODELLING

4.1 Overview

The accurate extraction of compensating signals has an imperative role in VSC control, representing its most significant aspect. The optimum output of the VSC relies heavily on the choice of the reference generation scheme. Various control schemes exist in both the time domain and frequency domain, as documented in the literature. Frequency-controlled methodologies suffer from the drawback of extended response times. On the other hand, time-domain techniques carry advantages such as simplistic in nature, ease of implementation, and reduced computational requirements. Effective operation of the VSC in grid system to improvise power quality (PQ) heavily relies on the selection of congruous control methodologies. This section is aimed at evaluating different control methodologies that have been employed to enhance the operation of VSCs.

4.2 Control Methodology

The proposed topology incorporates a two-step conversion architecture to integrate with a three-phase grid. The control scheme implemented aims to maximize power extraction from the solar power generating system (SPGS) and inject it into the grid at the PCC while maintaining power quality and ensuring overall system reliability and efficiency. The control strategy consists of two main components: the control mechanism for the Voltage Source Converter (VSC) and the generation of switching pulses using an indirect current control approach.

4.3 Determining Unit Templates and Terminal Voltage

The obtained line voltages (v_{XAB} , v_{XBC}) of the distribution feeder are subjected to a filtering process to diminish the impact of distortion and imbalances in the voltages of

distribution feeder. The observed line voltages are employed to determine the phase-to-neutral voltages (v_{XA}, v_{XB}, v_{XC}) [45].

$$\begin{bmatrix} v_{XA} \\ v_{XB} \\ v_{XC} \end{bmatrix} = (1/3) * \begin{bmatrix} 2 & 1 \\ -1 & 1 \\ -1 & 2 \end{bmatrix} * \begin{bmatrix} v_{XAB} \\ v_{XBC} \end{bmatrix} \quad (4.1)$$

The amplitude V_{TER} is computed using phase voltages as per eqn. (4.2),

$$V_{TER} = \sqrt{\left(\frac{2}{3}\right) * (v_{XA} + v_{XB} + v_{XC})} \quad (4.2)$$

Equation (4.3) gives the value of in-phase unit templates (u_A, u_B, u_C).

$$\begin{bmatrix} u_A \\ u_B \\ u_C \end{bmatrix} = \frac{1}{V_{TER}} \begin{bmatrix} v_{XA} \\ v_{XB} \\ v_{XC} \end{bmatrix} \quad (4.3)$$

4.4 Active Loss Weight (W_{DC}) component Extraction

The voltage error VSC DC-link is formulated below

$$V_{DC}^{Error}(p) = V_{DC}^{Ref}(p) - V_{DC}(p) \quad (4.4)$$

Voltage error of DC-link is symbolised as $V_{DC,}^{Error}$ whereas, representation of DC-link voltage of VSC is V_{DC}, and reference voltage is V_{DC}^{Ref} and respectively. In order to sustain DC-link voltage for VSC, V_{DC}^{Error} is incorporated in PI controller [45, 38]. It may be approximated as,

$$\begin{aligned} W_{DC}(P+1) = W_{DC}(P) &+ \chi_{in} V_{DC}{}^{Error}(p+1) \\ &+ \chi_{pr}\{V_{DC}^{Error}(p+1) \\ &- V_{DC}^{Error}(p)\} \quad (4.5) \end{aligned}$$

wherein $\chi_{Pr}$and $\chi_{in}$is proportional and integral gain of the PI controller respectively [45].

The estimated value of the SPV array's feed-forward component (W_{PV}) is

$$W_{SPV} = 2 * P_{SPV}(p)/3 * V_{TER} \quad (4.6)$$

P_{SPV} is the maximum power harvested from a SPV generation system [45].

4.5 Generating VSC Switching Pulses

Effective weight (W_{AVG}) can be summarized by the below given formula [45].

$$W_{AVG} = W_{LN} + W_{DC} - W_{SPV} \tag{4.7}$$

Reference grid current can be established with help of formula given below.

$$\begin{bmatrix} i_{XA}^{Ref} \\ i_{XB}^{Ref} \\ i_{XC}^{Ref} \end{bmatrix} = W_{AVG} \begin{bmatrix} u_A \\ u_B \\ u_C \end{bmatrix} \tag{4.8}$$

Indirect control is used in conjunction with a hysteresis controller to enable switching of the VSC. It is possible to figure out the current error by comparing reference ($i_{XA}^{Ref}, i_{XB}^{Ref}, i_{XC}^{Ref}$) measured ($i_{GA}$, i_{GB}, i_{GC}) grid currents. Hysteresis controller uses such erroneous signals as input to generate a broad spectrum of gate pulses.

4.6 Least Mean Square (LMS) based Adaptive Algorithm

Reduced computational complexity, easy to implement and enhanced steady state performance gives an edge to zero attraction topology over other control algorithms. Few of the Zero Attracting Least Mean Square based techniques are, the Robust ZA-LMS (RZA-LMS) technique, the polynomial zero-attraction (PZA)-LMS control algorithm the l_0-LMStechnique and the ZA-LMS technique.

Recursive updating of the weight of a model is experienced in zero-attracting algorithm based on LMS criterion, some cost function, which persists due to l_2 norms and approximated l_0 norms of $\mathcal{E}(p)$ and $W_{LN}(p)$ respectively, are eliminated and updated weight is expressed as

$$W_{LN}(p+1) = W_{LN}(p) + \mu u(p)[\mathcal{E}_C(p)] - \rho * \psi'_{l0} \tag{4.9}$$

ψ_{l0} is a function, and approximates l_0 norms of a weight $W_{LN}(p)$.

ψ'_{l0} is the derivative of ψ_{l0}, ρ is zero-attracting parameter which is taken as more than zero [47-49].

Some of the adaptive methods based on LMS is explained and developed are listed below.

1- Least Mean Square (LMS) algorithm

2- Zero-Attracting-LMS algorithm

3- Robust Zero Attraction-LMS algorithm

4- Modified Versoria based Zero attraction- LMS (MVZ-LMS)

4.7 Least Mean Square (LMS) based Control algorithm

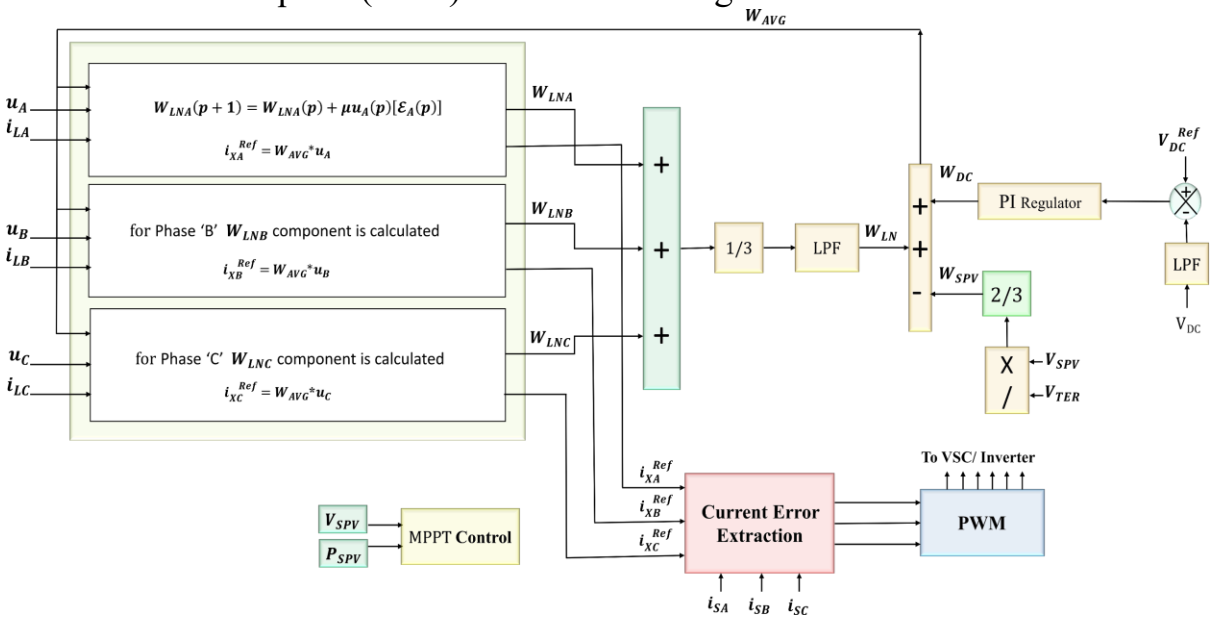

Fig. 4.1 LMS based control Architecture

4.7.1 Weight Component linked to loads (W_{LN})

Load weight component is assessed by employing the LMS model.

The load current (i_{LA}) in phase "A" has a weight factor denoted by W_{LNA} may be assessed as follows

$$W_{LNA}(p+1) = W_{LNA}(p) + \mu u_A(p)[\mathcal{E}_A(p)] \tag{4.10}$$

Where, μ is the step size.

$\mathcal{E}_A(p)$ is error, and calculated as

$$\mathcal{E}_A(p) = i_{LA}(P) - W_{LNA}(P) * u_A(p) \tag{4.11}$$

Accordingly, Weight components of "B" and "C" phases will be computed by applying equations (4.12) and (4.13) respectively.

$$W_{LNB}(p+1) = W_{LNB}(p) + \mu u_B(p)[\mathcal{E}_B(p)] \tag{4.12}$$

$$W_{LNC}(p+1) = W_{LNC}(p) + \mu u_C(p)[\mathcal{E}_C(p)] \tag{4.13}$$

Mean linked load (W_{LP}) weight factor is ascertained by,

$$W_{LN} = \frac{1}{3}(W_{LNA} + W_{LNB} + W_{LNC}) \tag{4.14}$$

4.8 Zero Attraction-LMS based control Algorithm

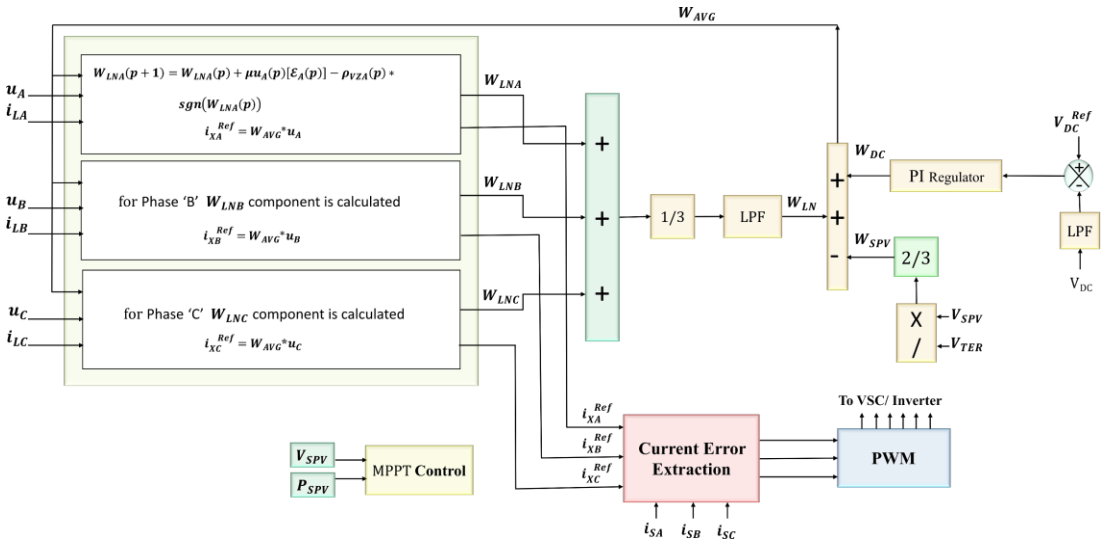

Fig. 4.2 ZA-LMS based control Algorithm

4.8.1 Weight Component linked to loads (W_{LN})

Loads weight component is assessed by employing ZA-LMS model. The expressed LMS model incorporates a penalty factor based on the zero-attraction to provide enhanced zero-attraction potential.

The load current (i_{LA}) in phase "A" has a weight factor denoted by W_{LNA} may be assessed as follows

$$W_{LNA}(p+1) = W_{LNA}(p) + \mu u_A(p)[\mathcal{E}_A(p)] - \rho_{VZA}(p) * sgn\big(W_{LPA}(p)\big) \tag{4.15}$$

μ is the step size and $\rho_{VZA}(p) * sgn\big(W_{LPA}(p)\big)$ is a zero-attraction component.

$\mathcal{E}_A(p)$ is error and calculated as,

$$\mathcal{E}_A(p) = i_{LA}(P) - W_{LNA}(P) * u_A(p) \tag{4.16}$$

Accordingly, Weight components of "B" and "C" phases will be computed by applying equations (4.17) and (4.18) respectively.

$$W_{LNB}(p+1) = W_{LNB}(p) + \mu u_B(p)[\mathcal{E}_B(p)] - \rho_{VZB}(p) * sgn\big(W_{LPB}(p)\big) \tag{4.17}$$

$$W_{LNC}(p+1) = W_{LNC}(p) + \mu u_C(p)[\mathcal{E}_C(p)] - \rho_{VZC}(p) * sgn\big(W_{LPC}(p)\big) \tag{4.18}$$

Mean linked load (W_{LP}) weight factor is ascertained by,

$$W_{LN} = \frac{1}{3}(W_{LNA} + W_{LNB} + W_{LNC}) \tag{4.19}$$

4.9 Robust Zero Attraction-LMS based control Algorithm

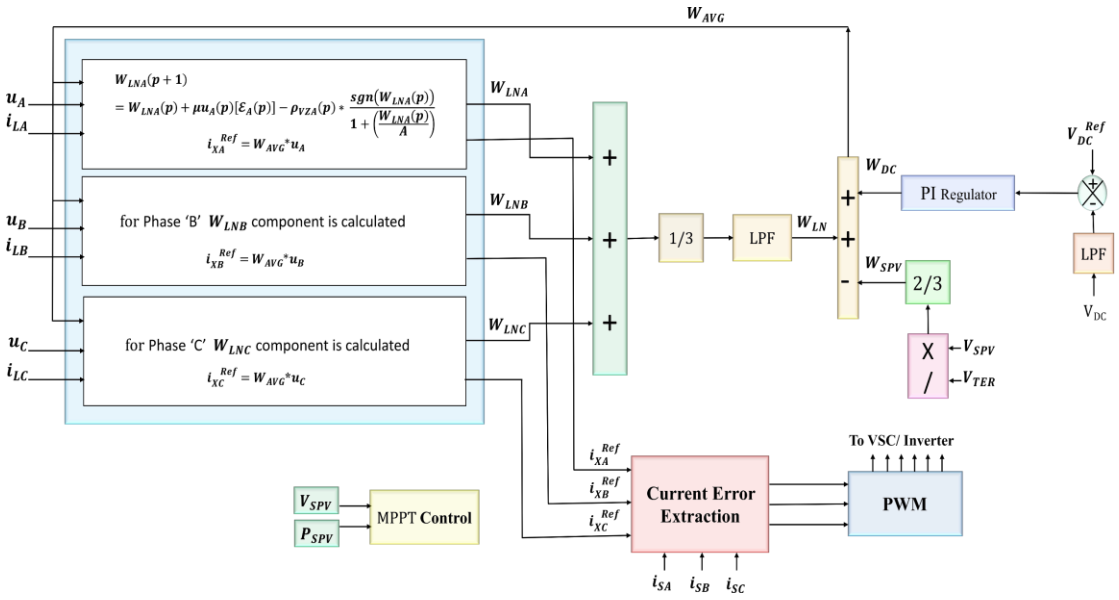

Fig. 4.3 RZA-LMS based control Algorithm

4.9.1 Weight Component linked to loads (W_{LN})

Loads weight component is assessed by employing the RZA-LMS model, which has an improved zero component attraction capability and hence, better accuracy than ZA-LMS [52, 49].

The load current (i_{LA}) in phase "A" has a weight factor denoted by W_{LNA} may be assessed as follows

$$W_{LNA}(p+1) = W_{LNA}(p) + \mu u_A(p)[\mathcal{E}_A(p)] - \rho_{VZA}(p) * \frac{sgn(W_{LPA}(p))}{1+\left(\frac{W_{LPA}(p)}{A}\right)} \tag{4.20}$$

μ is the step size and $\rho_{VZA}(p) * \frac{sgn(W_{LPA}(p))}{1+\left(\frac{W_{LPA}(p)}{A}\right)}$ is a zero-attraction component.

$\mathcal{E}_A(p)$ is error and calculated as,

$$\mathcal{E}_A(p) = i_{LA}(P) - W_{LN}(P) * u_A(p) \tag{4.21}$$

Accordingly, Weight components of "B" and "C" phases will be computed by applying equations (4.22) and (4.23) respectively.

$$W_{LNB}(p+1) = W_{LNB}(p) + \mu u_B(p)[\mathcal{E}_B(p)] - \rho_{VZB}(p) * \frac{sgn(W_{LPB}(p))}{1+\left(\frac{W_{LPB}(p)}{A}\right)} \tag{4.22}$$

$$W_{LNC}(p+1) = W_{LNC}(p) + \mu u_C(p)[\mathcal{E}_C(p)] - \rho_{VZC}(p) * \frac{sgn(W_{LPC}(p))}{1+\left(\frac{W_{LPC}(p)}{A}\right)} \tag{4.23}$$

Mean linked load (W_{LP}) weight factor is ascertained by,

$$W_{LN} = \frac{1}{3}(W_{LNA} + W_{LNB} + W_{LNC}) \tag{4.24}$$

4.10 Modified Versoria based- ZALMS Control Algorithm

Equation 4.25 defines the Versoria function [49].

$$f[W_{LN}(p)] = \frac{A^3}{A^2 + (W_{LP}(p))^2} \tag{4.25}$$

As A ≥ 0, which is a constant.

Behavior of the Versoria Function (VF) is consistently non-increasing for every value of $W_{LN}(p) \geq 0$, as desired feature of ψ'_{l0}.VF cannot be used directly as a penalty factor, as seen from equation (4.9), so if, VF in its original form is incorporated in the LMS, negative $W_{LN}(p)$ values will be added and will move away from zero, which is a non-desirable feature and jeopardized the very logic of zero-attraction [47, 48]. Therefore, to use VF as a penalty factor, normalization of the VF is carried out by inducting a $sgn(\cdot)$ term in the basic VF and hence, modified VF can be developed, which fulfill all the necessary conditions to act as a zero-attracting algorithm [47-49].

$$f[W_{LN}(p)] = sgn[W_{LN}(p)] * \frac{A^3}{A^2+\left(W_{LP}(p)\right)^2} = A_1 * \frac{sgn(W_{LPA}(p))}{1+\left(\frac{W_{LPA}(p)}{A}\right)^2} \tag{4.26}$$

Where $A_1$is a constant and A_1 equals A for basic VF.

Selectivity of the proposed techniques is enhanced because of non- linear characteristics of the penalty factor, which attracts near-zero coefficient in the short range, which improves the performance of the proposed algorithm in comparison to other [47].

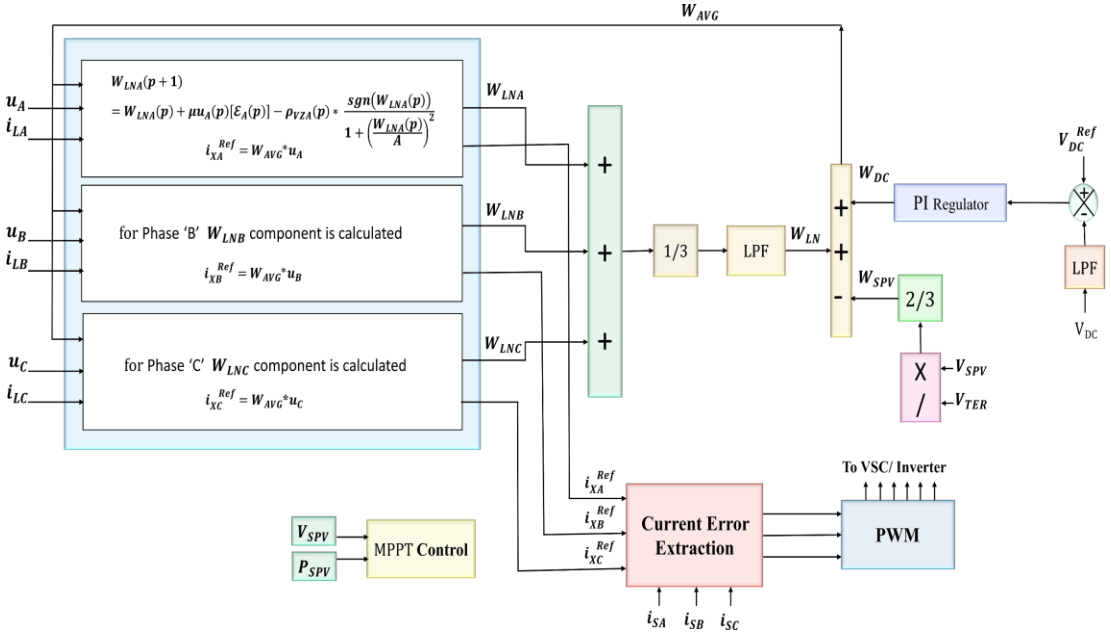

Fig. 4.4 Modified Versoria based ZA-LMS based control Algorithm

4.10.1 Weight Component linked to loads (W_{LN})

Loads weight component is assessed by employing the suggested MVZA-LMS model. The expressed LMS model incorporates a penalty factor based on the Versoria function to provide enhanced zero-attraction potential, which will lead to reduce computing complexity, higher modelling precision, quick and efficient convergence, and improved dynamic performance in severely deformed circumstances [47-49].

The load current (i_{LA}) in phase "A" has a weight factor denoted by W_{LNA} may be assessed as follows

$$W_{LNA}(p+1) = W_{LNA}(p) + \mu u_A(p)[\mathcal{E}_A(p)] - \rho_{VZA}(p) * \frac{sgn(W_{LPA}(p))}{1+\left(\frac{W_{LPA}(p)}{A}\right)^2} \quad (4.27)$$

μ is the step size and $\rho_{VZA}(p) * \frac{sgn(W_{LPA}(p))}{1+\left(\frac{W_{LPA}(p)}{A}\right)^2}$ is a zero-attraction component.

$\mathcal{E}_A(p)$ is error and calculated as,

$$\mathcal{E}_A(p) = i_{LA}(P) - W_{LNA}(P) * u_A(p) \quad (4.28)$$

Accordingly, Weight components of "B" and "C" phases will be computed by applying equations (4.21) and (4.22) respectively.

$$W_{LNB}(p+1) = W_{LNB}(p) + \mu u_B(p)[\mathcal{E}_B(p)] - \rho_{VZB}(p)\frac{sgn\left(W_{LPB}(p)\right)}{1+\left(\frac{W_{LPB}(p)}{A}\right)^2} \quad (4.29)$$

$$W_{LNC}(p+1) = W_{LNC}(p) + \mu u_C(p)[\mathcal{E}_C(p)] - \rho_{VZC}(p) * \frac{sgn\left(W_{LPC}(p)\right)}{1+\left(\frac{W_{LPC}(p)}{A}\right)^2} \quad (4.30)$$

Mean linked load (W_{LP}) weight factor is ascertained by

$$W_{LN} = \frac{1}{3}(W_{LNA} + W_{LNB} + W_{LNC}) \quad (4.31)$$

CHAPTER 5

SIMULATION AND RESULTS

5.1 Simulation of the VSC control Algorithm Model

This research work utilizes the MATLAB Simulink environment to simulate various control algorithms, including the proposed MVZA-LMS, RZA-LMS, ZA-LMS, and LMS. The objective is to assess their response under time-varying conditions, such as fluctuations in solar irradiance and the presence of nonlinear unbalanced loads.

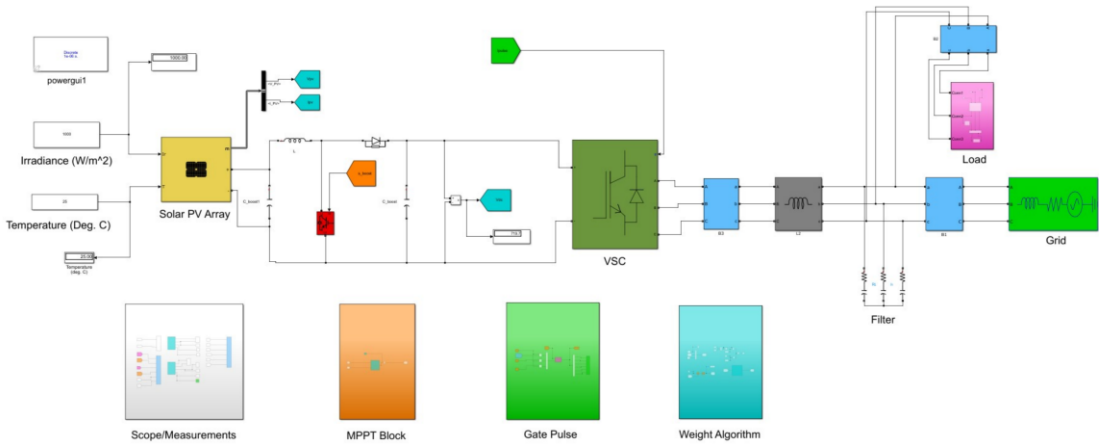

Fig. 5.1 Simulink Model of a 44 kW, 3-phase, Double Stage Grid-tied System

5.2 Response of the System under Non-linear Unbalanced Load conditions

In order to study the behaviour of an unbalanced non-linear load condition, phase 'B' (I_{LB}) was intentionally disconnected and reconnected at 0.4 and 0.6 seconds, respectively, as depicted in Figure 5.2. When the load is disconnected at 0.4 seconds, the power demanded by the load decreases, resulting in an increase in grid current (I_G). Consequently, as shown in Figures 5.3,5.5,5.7,5.9 (a) power (P_G) is fed back to the grid. By implementing compensation in the suggested Voltage Source Converter control, the grid current at the point of common coupling (PCC) is effectively balanced and sinusoidal. Figures 5.3,5.5,5.7,5.9 (b) demonstrates that the solar PV array operates at the maximum power point (I_{SPV} and V_{SPV}) with a stable DC link voltage (V_{DC}) during the load unbalancing phase. Although the load component (W_{LN}) decreases due to the

overall reduction in load, the velocity component (W_{SPV}) remains constant, resulting in a decrease in the effective weight (W_{AVG}).

As shown in Figure 5.4, the VSC current (I_{INV}), grid voltage (V_G), load current (I_{LB}), and grid current (I_G) exhibit total harmonic distortions (THD) of 6.60%, 0.03%, 23.63%, and 1.06%, respectively for the proposed algorithm. After load balancing, the THD percentage of the grid current demonstrates compliance within the permissible boundaries set by the IEEE-519 standard [53].

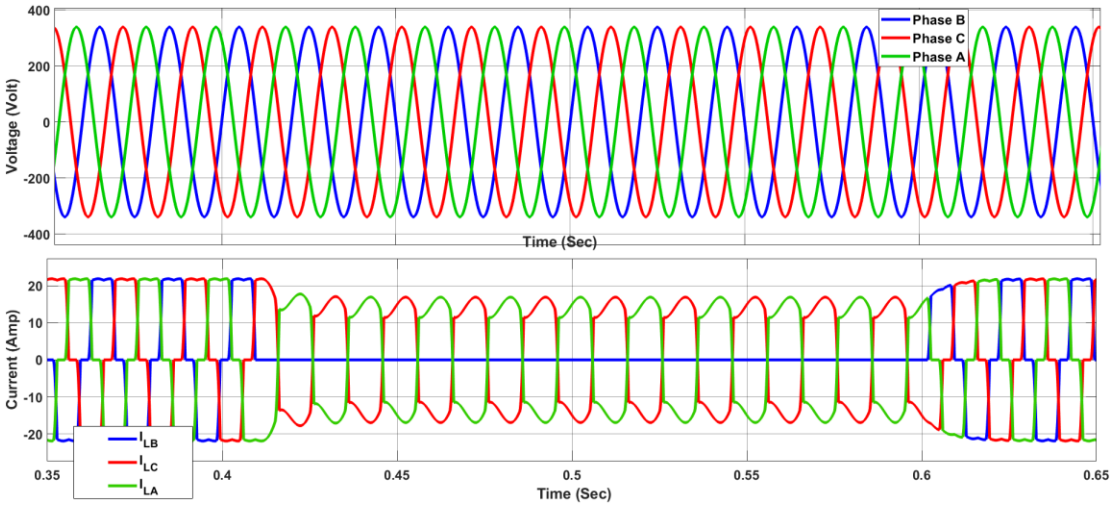

Fig.5.2 Three -phase Voltage (V) and Load Current (A)

5.2.1 LMS Algorithm

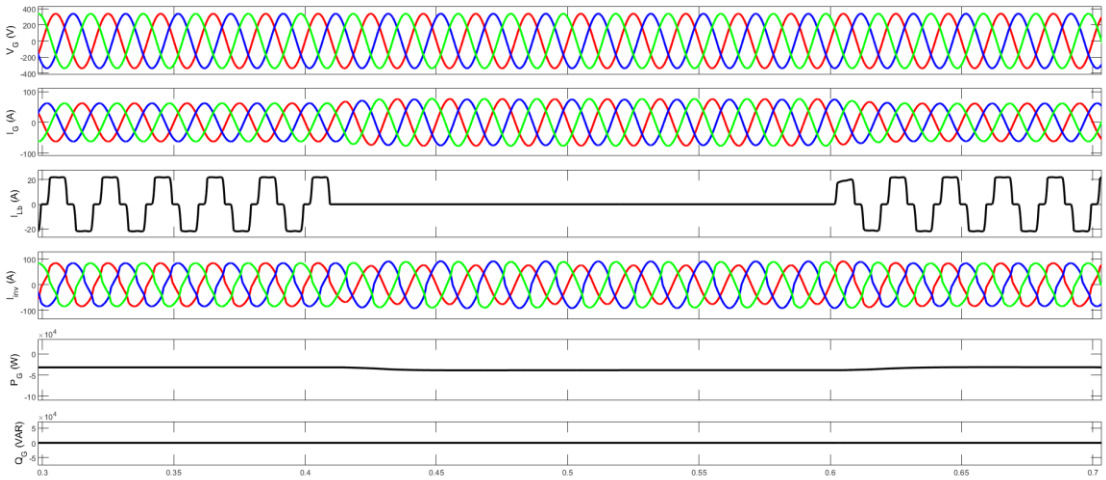

(a)

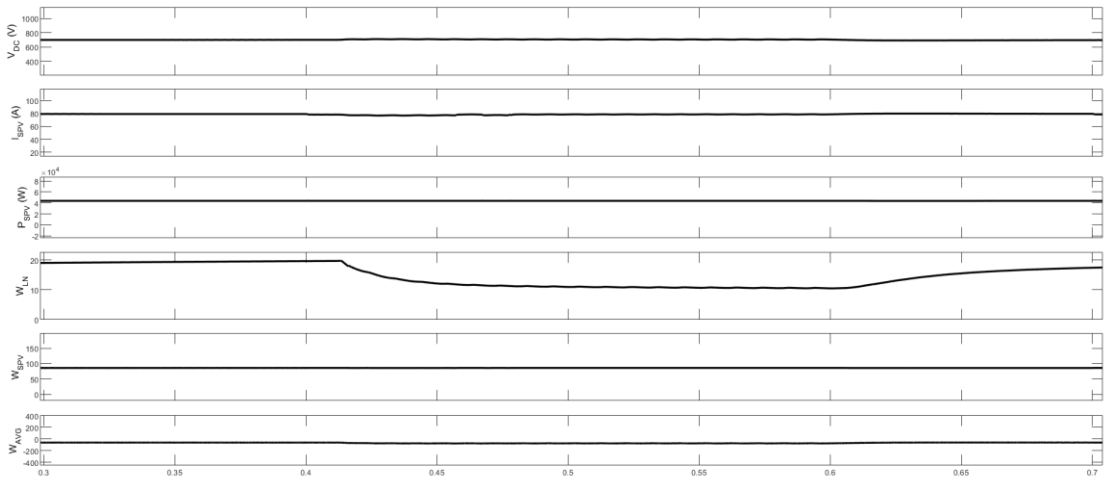

(b)

Fig 5.3 Response of the model for unbalanced non-linear load for LMS-algorithm (a) includes Grid voltage (V_G), Grid current (I_G), Load current (I_L), Inverter current (I_{INV}), Active Grid Power (P_G) in Watt and Reactive Grid power (Q_G) in VAR (b) includes DC voltage (V_{DC}), PV power (P_{SPV}), PV current, and weight components W_{LN}, W_{DC} and W_{AVG}

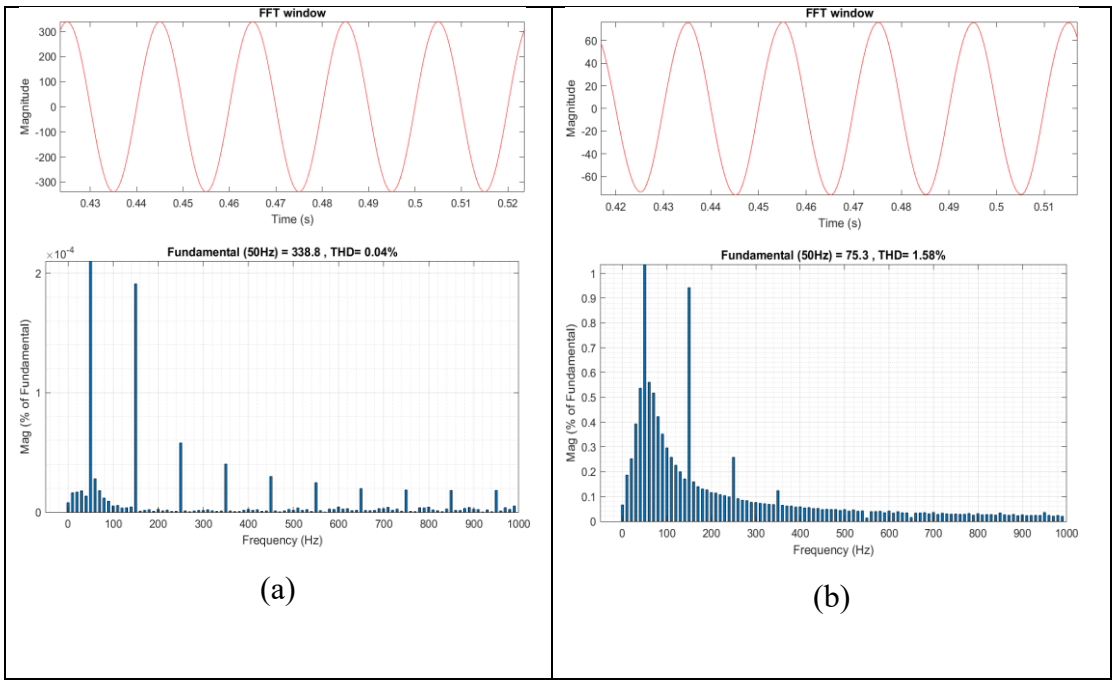

(a) (b)

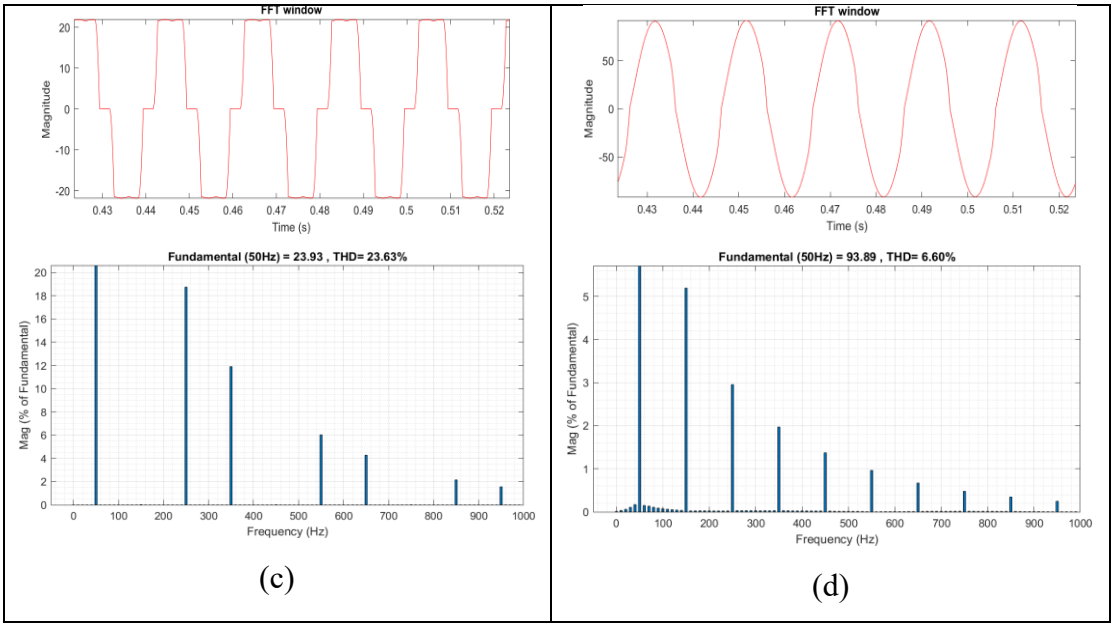

Fig 5.4 Harmonic spectrum using LMS control methodology for the unbalanced non-linear load and its THD (a) Grid voltage (V_G) %THD and magnitude (b) Grid current (I_G) %THD and magnitude (c) Load Current (I_{LB}) %THD and magnitude (d) Inverter Current (I_{inv}) %THD and magnitude.

5.2.2 ZA-LMS Algorithm

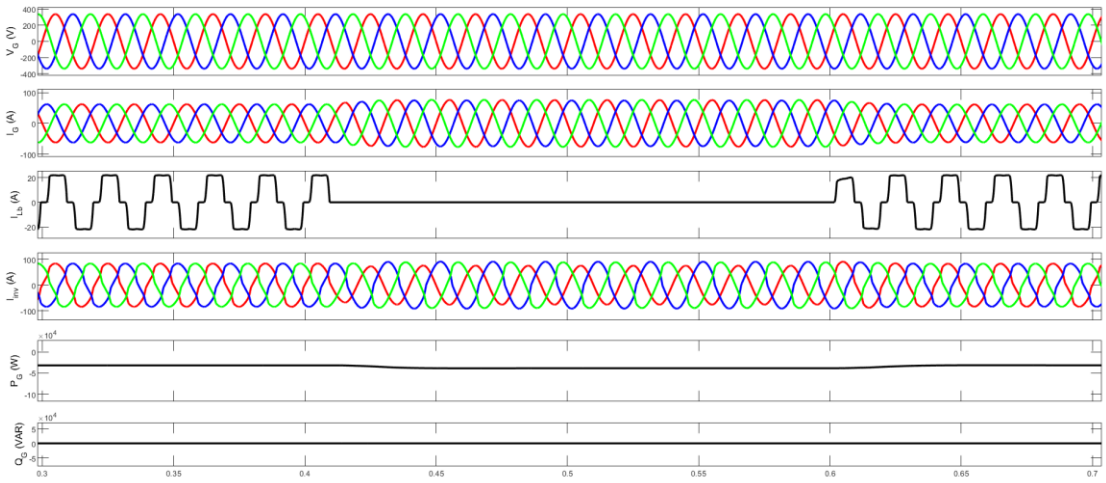

(a)

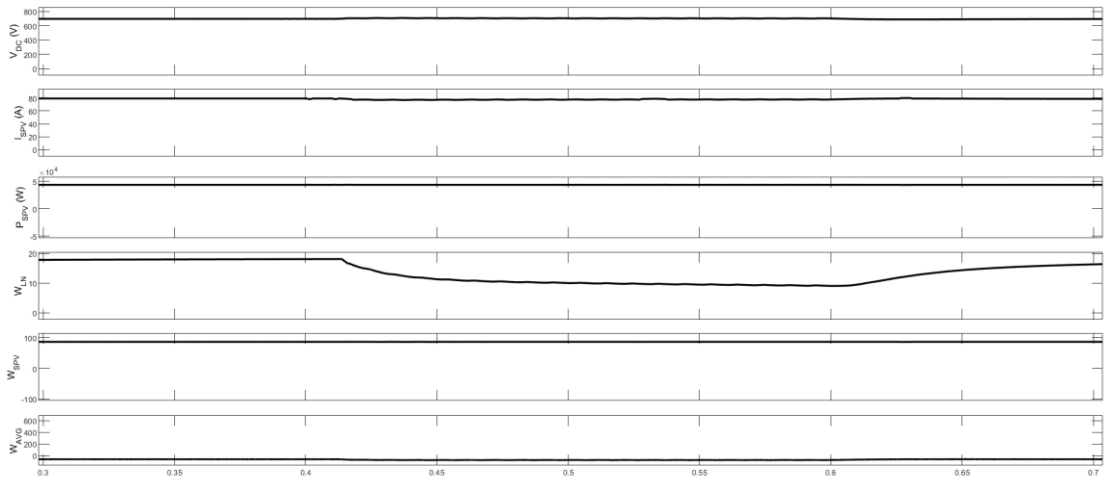

(b)

Fig 5.5 Response of the model for unbalanced non-linear load for ZA- LMS algorithm (a) includes Grid voltage (V_G), Grid current (I_G), Load current (I_L), Inverter current (I_{INV}), Active Grid Power (P_G) in Watt and Reactive Grid power (Q_G) in VAR (b) includes DC voltage (V_{DC}), PV power (P_{SPV}), PV current, and weight components W_{LN}, W_{DC} and W_{AVG}

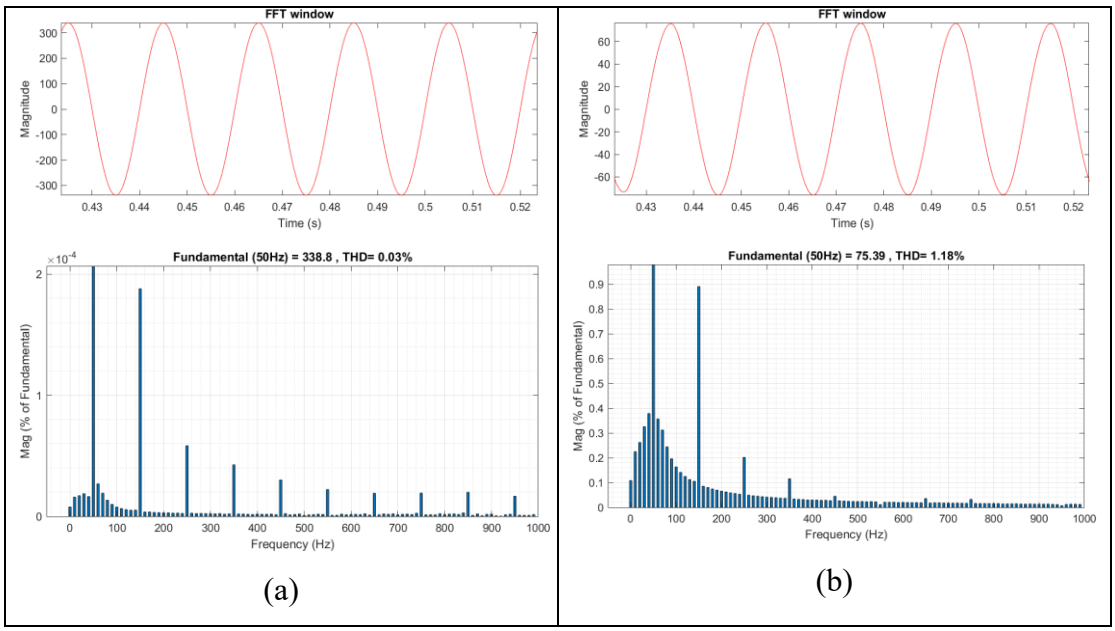

(a) (b)

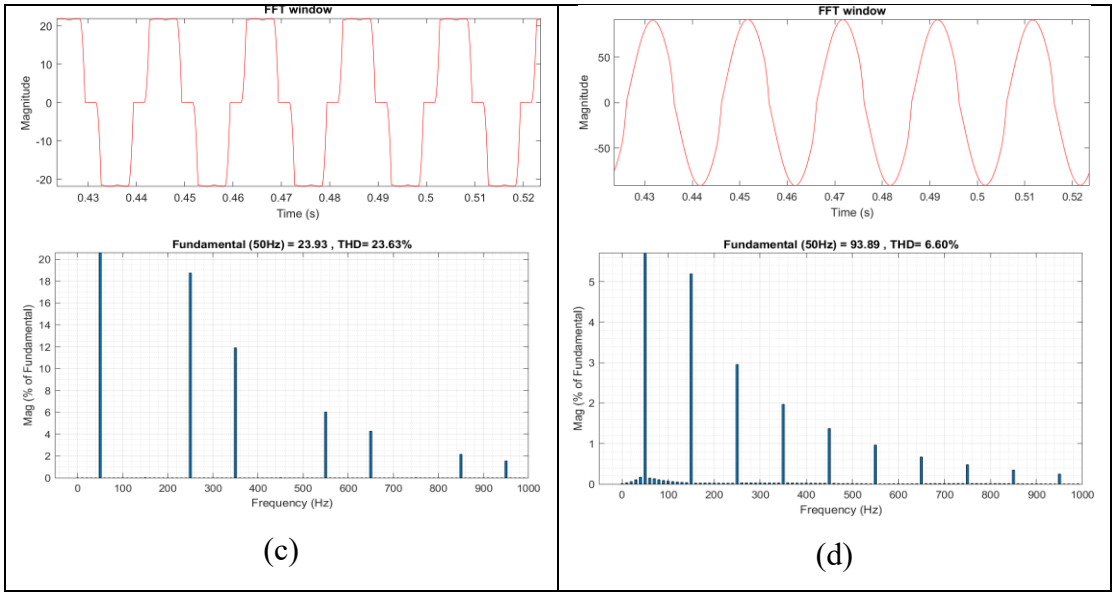

Fig 5.6 Harmonic spectrum using LMS control methodology for the unbalanced non-linear load and its THD (a) Grid voltage (V_G) %THD and magnitude (b) Grid current (I_G) %THD and magnitude (c) Load Current (I_{LB}) %THD and magnitude (d) Inverter Current (I_{inv}) %THD and magnitude.

5.2.3 RZA-LMS Algorithm

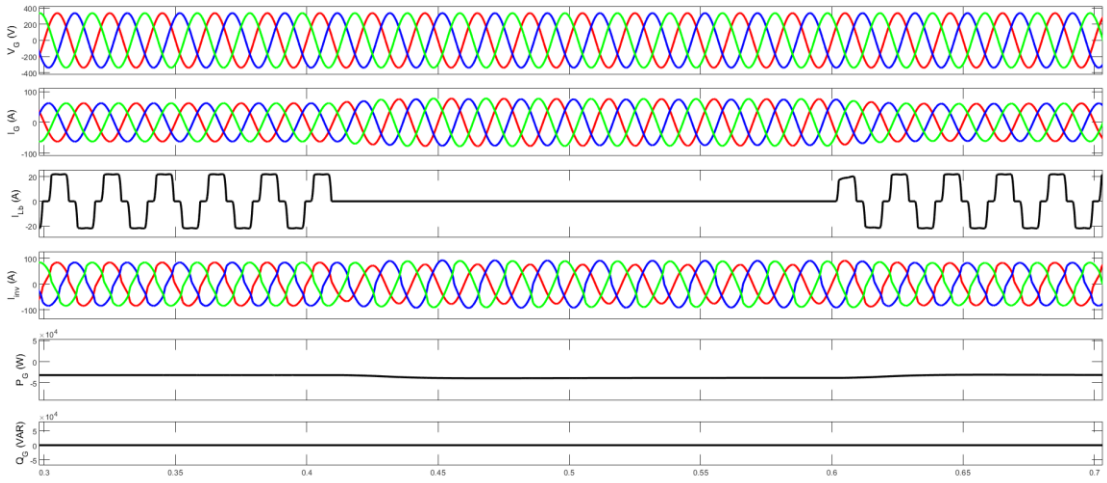

(a)

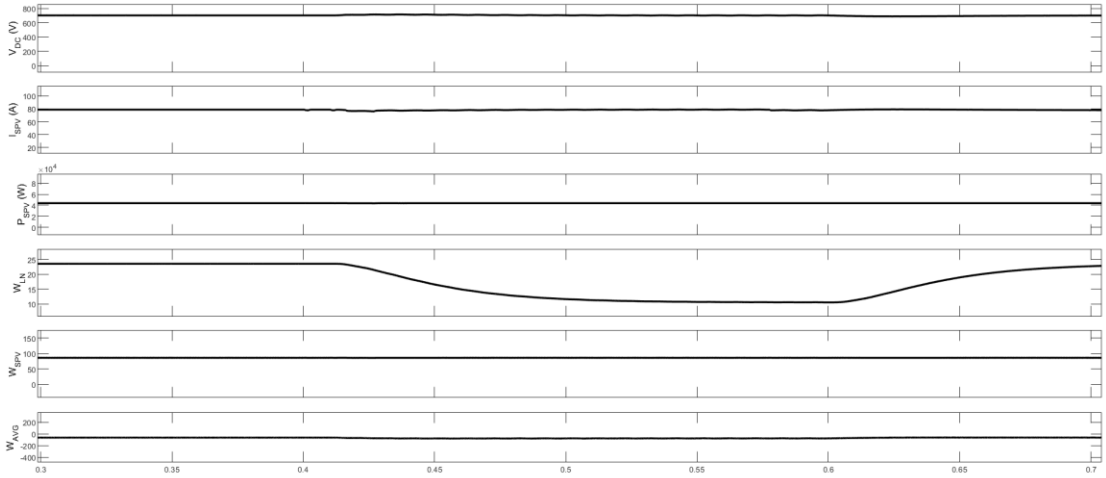

(b)

Fig 5.7 Response of the model for unbalanced non-linear load for LMS-algorithm (a) includes Grid voltage (V_G), Grid current (I_G), Load current (I_L), Inverter current (I_{INV}), Active Grid Power (P_G) in Watt and Reactive Grid power (Q_G) in VAR (b) includes DC voltage (V_{DC}), PV power (P_{SPV}), PV current, and weight components W_{LN}, W_{DC} and W_{AVG}

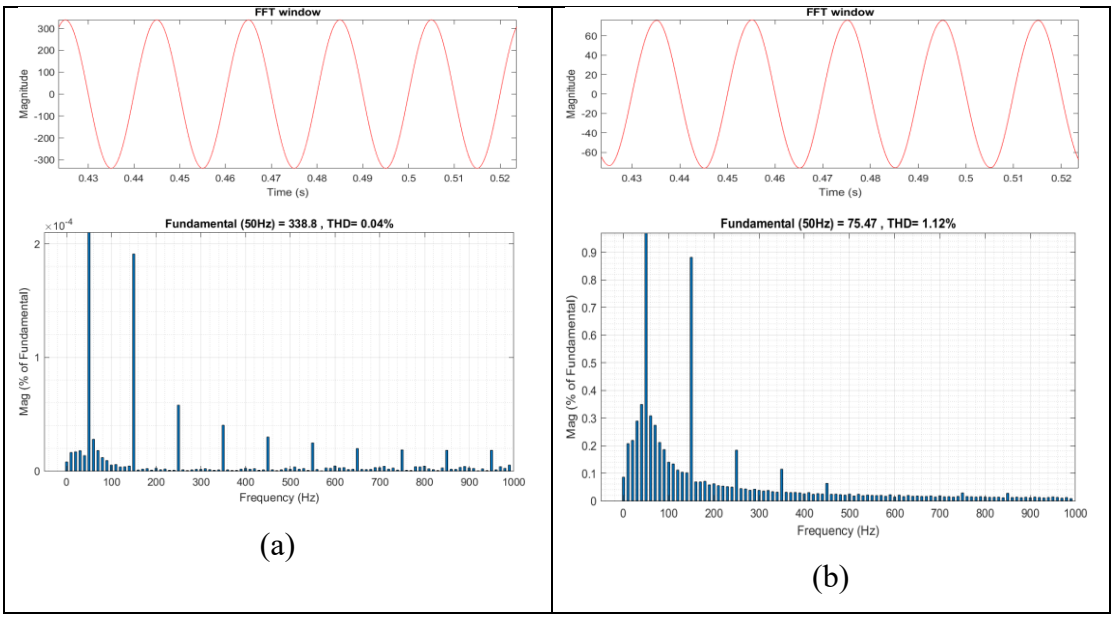

(a) (b)

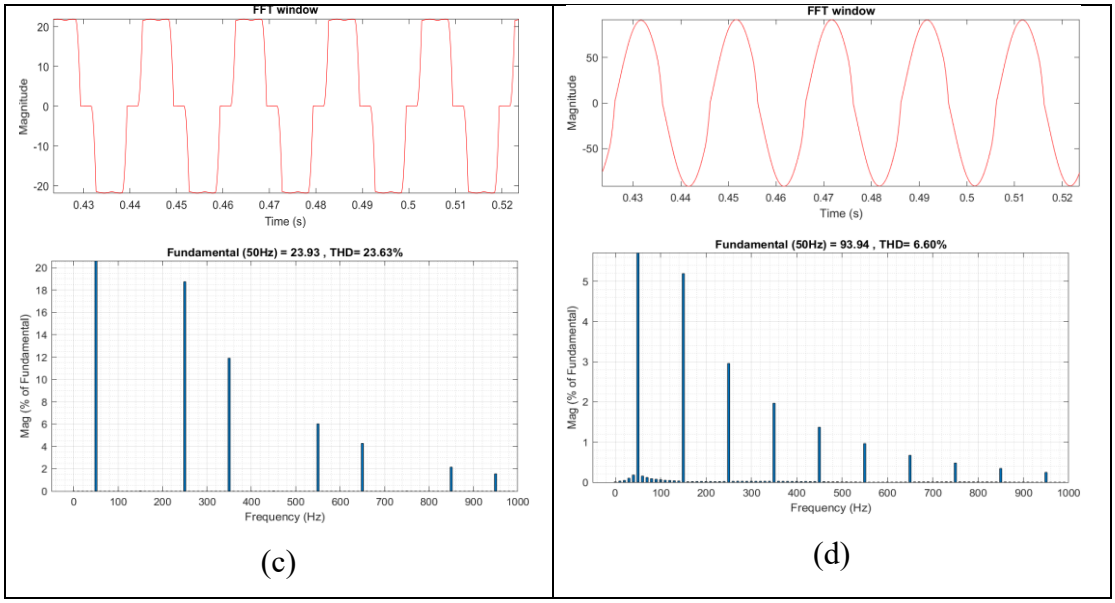

Fig 5.8 Harmonic spectrum using LMS control methodology for the unbalanced non-linear load and its THD (a) Grid voltage (V_G) %THD and magnitude (b) Grid current (I_G) %THD and magnitude (c) Load Current (I_{LB}) %THD and magnitude (d) Inverter Current (I_{inv}) %THD and magnitude.

5.2.4 MVZA-LMS

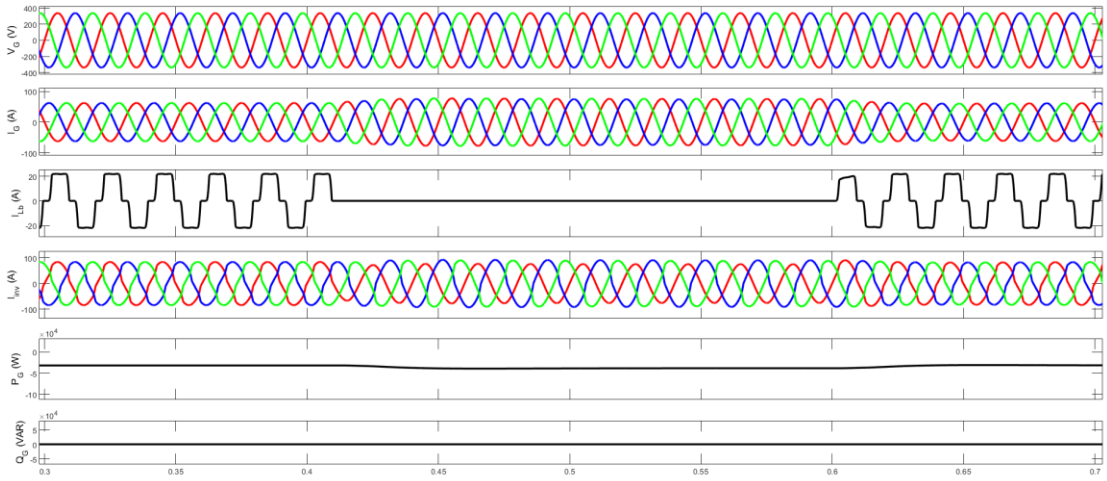

(a)

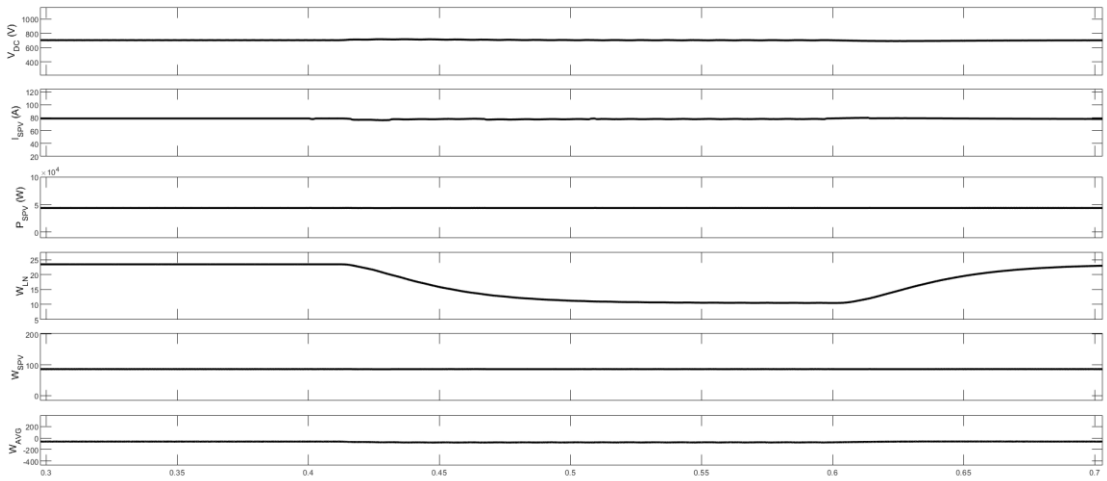

(b)

Fig. 5.9 Response of the model for unbalanced non-linear load for LMS-algorithm (a) includes Grid voltage (V_G), Grid current (I_G), Load current (I_L), Inverter current (I_{INV}), Active Grid Power (P_G) in Watt and Reactive Grid power (Q_G) in VAR (b) includes DC voltage (V_{DC}), PV power (P_{SPV}), PV current, and weight components W_{LN}, W_{DC} and W_{AVG}

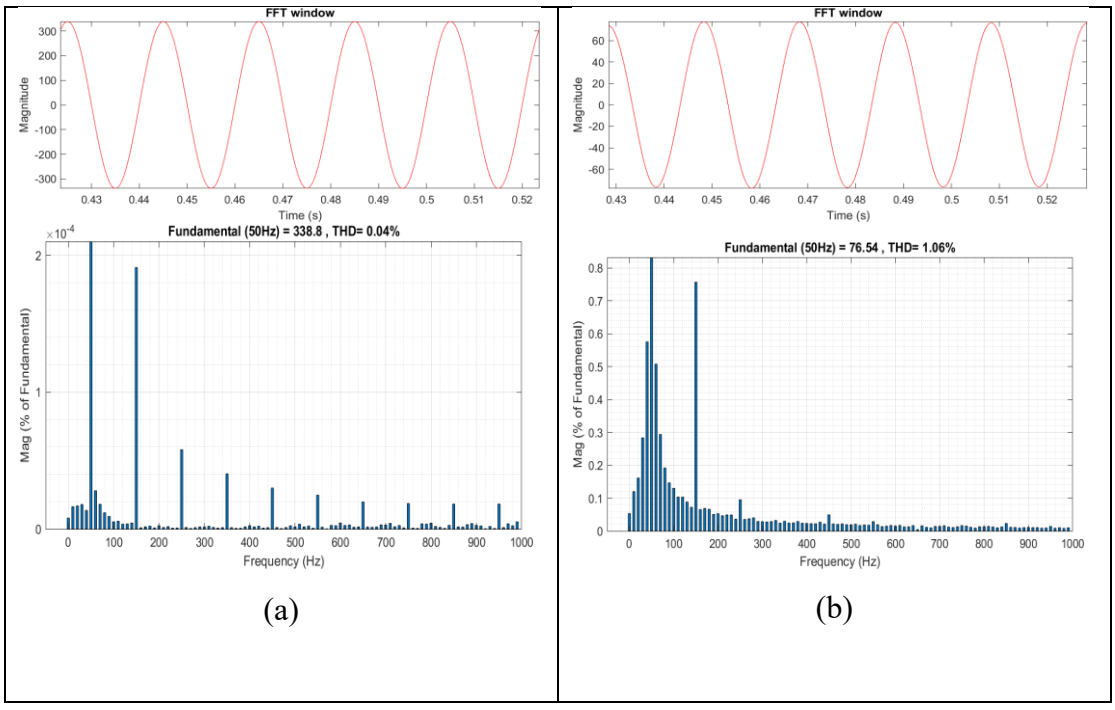

(a) (b)

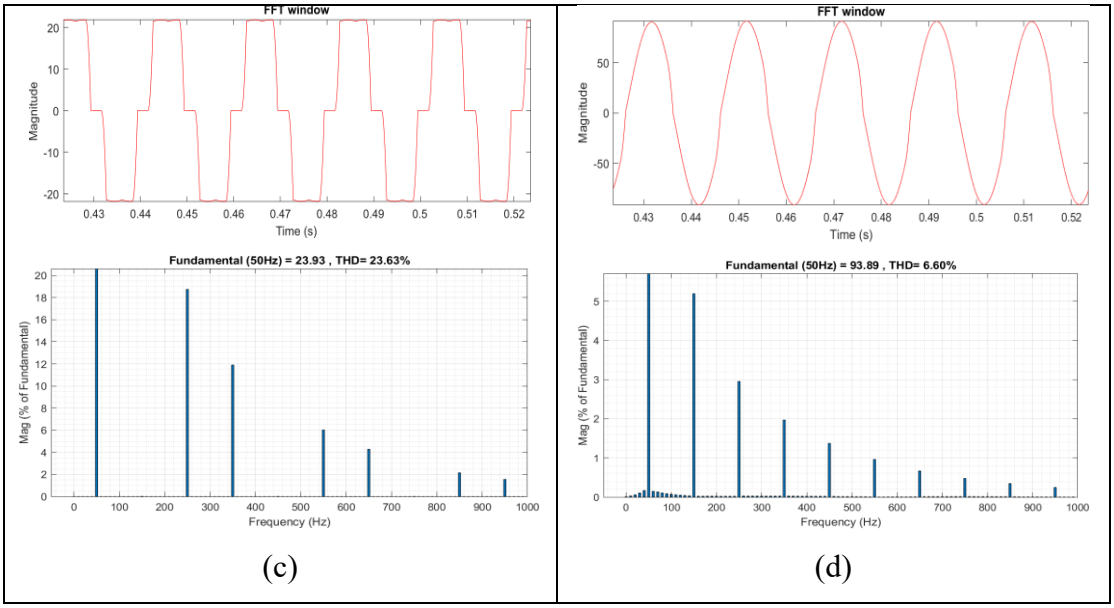

Fig 5.10 Harmonic spectrum using LMS control methodology for the unbalanced non-linear load and its THD (a) Grid voltage (V_G) %THD and magnitude (b) Grid current (I_G) %THD and magnitude (c) Load Current (I_{LB}) %THD and magnitude (d) Inverter Current (I_{inv}) %THD and magnitude.

5.3 Response of the System Under Variable Solar Insolation

Figures 5.11-5.14 demonstrates the response to changes in solar irradiation. At t = 0.4 to 0.6 seconds, the solar irradiation (Irr) is reduced from 1000 to 550 W/m^2. As a result of the decrease in solar PV-generated power (SPGS) being fed into the grid, both the grid current (I_G) and grid power (P_G) decrease, as depicted in Figure 5.11-5.14 (a). The grid current remains sinusoidal and balanced. Figure 5.11-5.14 (b) shows the PV array operating at its adjusted maximum power point (I_{PV} and V_{PV}), while maintaining a stable DC-link voltage (V_{DC}). The load weight factor (W_{LN}) remains unchanged, but the weight component (W_{PV}) improves due to the reduction in SPV power, resulting in an increase in the average weight (W_{AVG}).

5.3.1 LMS Algorithm under variable Insolation

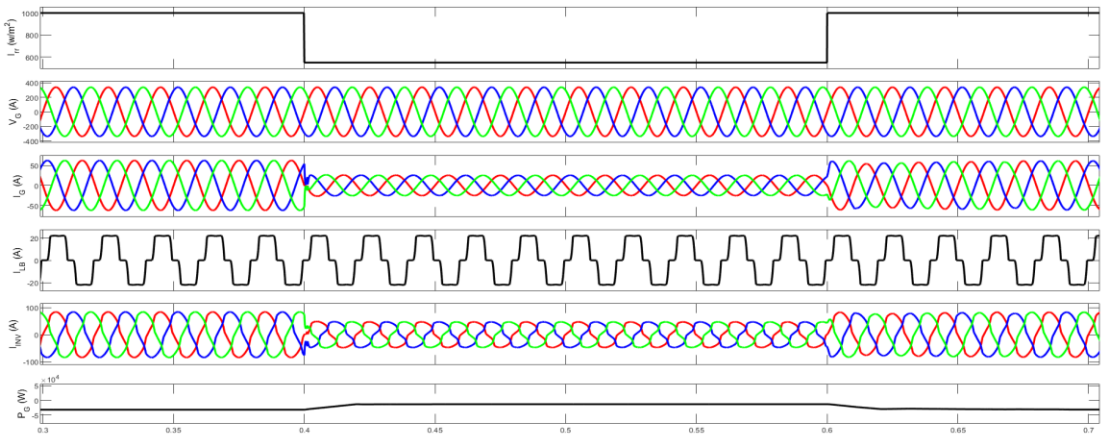

(a)

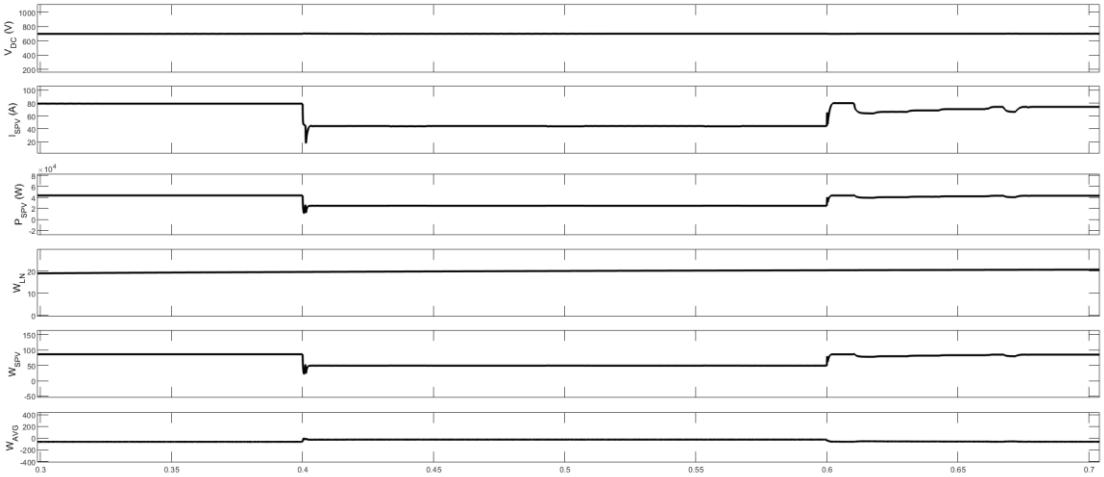

(b)

Fig. 5.11 (a) Shows the behavior of Solar irradiance (Irr), Grid voltage (VG), Grid current (IG), Inverter current (Iinv) and Grid power (P_G). (b) shows the characteristics of VDC, I_{SPV}, P_{SPV}, Weight component of load (W_{LN}), PV weight Component (W_{SPV}) and Average weight (W_{AVG}).

5.3.2 Varying irradiance ZA-LMS algorithm

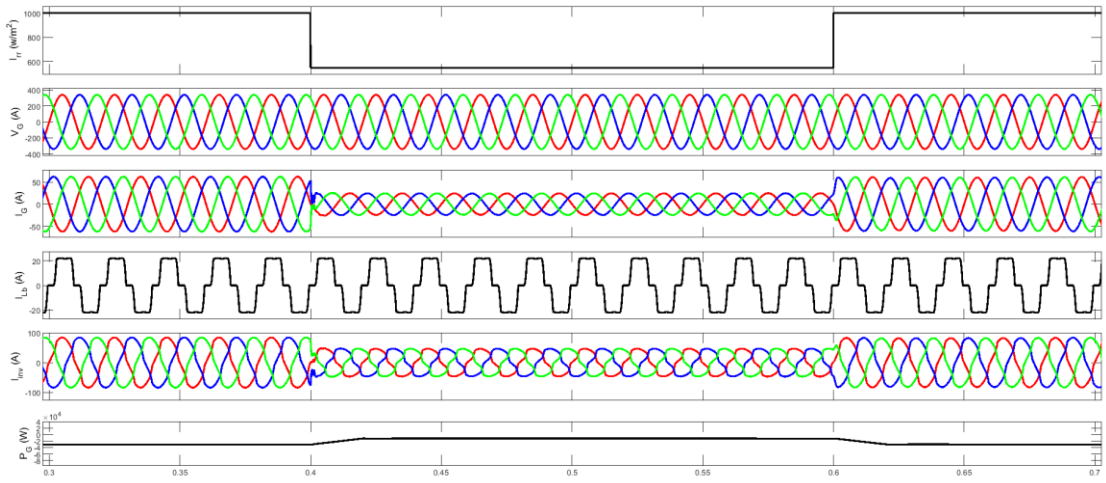

(a)

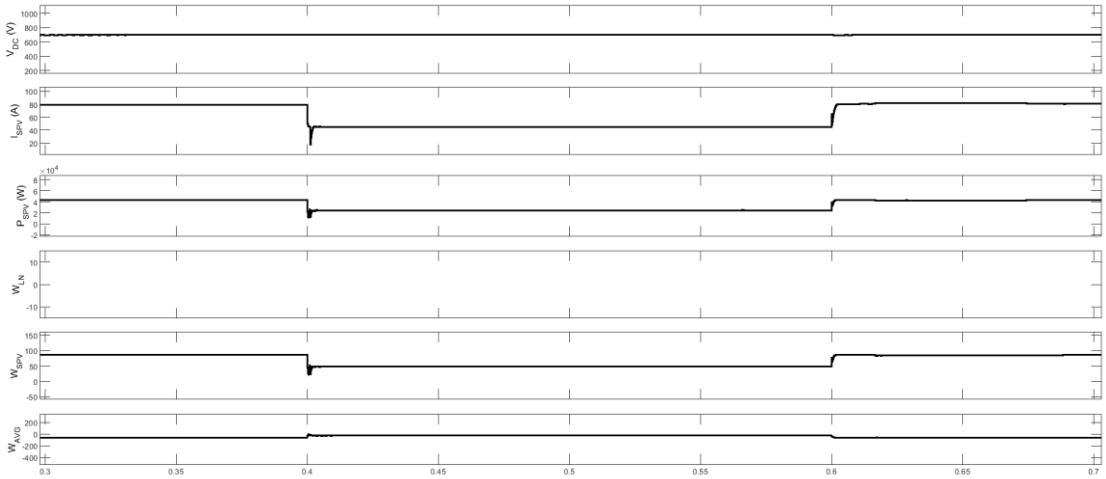

(b)

Fig. 5.12 (a) Shows the behavior of Solar irradiance (Irr), Grid voltage (VG), Grid current (IG), Inverter current (Iinv) and Grid power (P_G). (b) shows the characteristics of VDC, I_{SPV}, $P_{SPV,}$ Weight component of load (W_{LN}), PV weight Component (W_{SPV}) and Average weight (W_{AVG}).

5.3.3 Varying irradiance RZA-LMS algorithm

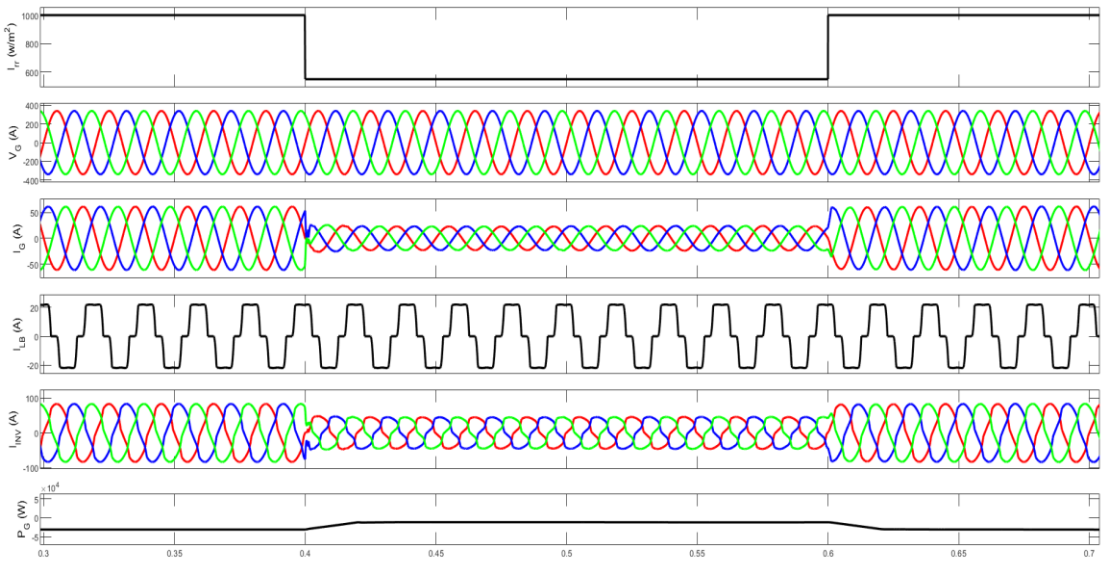

(a)

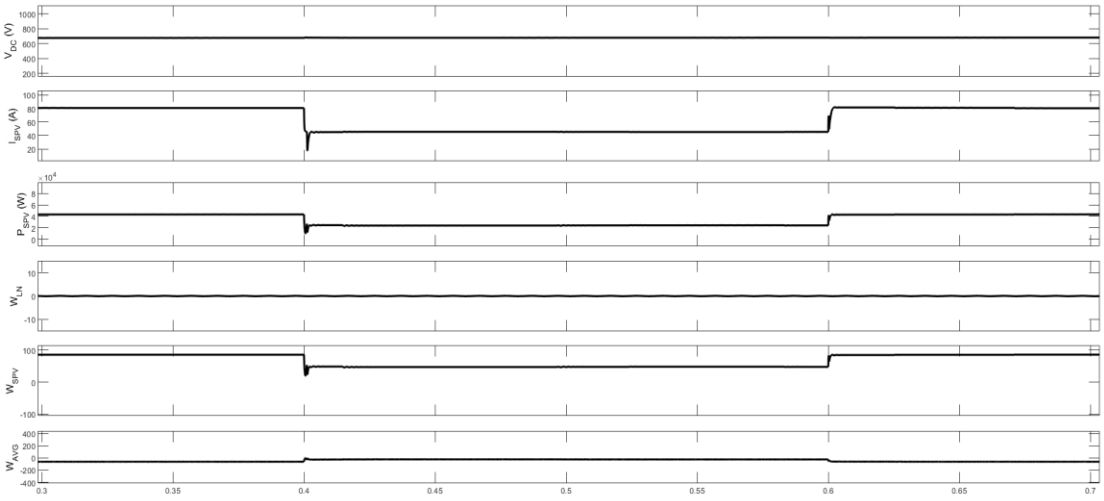

(b)

Fig. 5.13 (a) Shows the behavior of Solar irradiance (Irr), Grid voltage (VG), Grid current (IG), Inverter current (Iinv) and Grid power (P_G). (b) shows the characteristics of VDC, I_{SPV}, $P_{SPV,}$ Weight component of load (W_{LN}), PV weight Component (W_{SPV}) and Average weight (W_{AVG}).

5.3. Varying irradiance MVZA-LMS algorithm

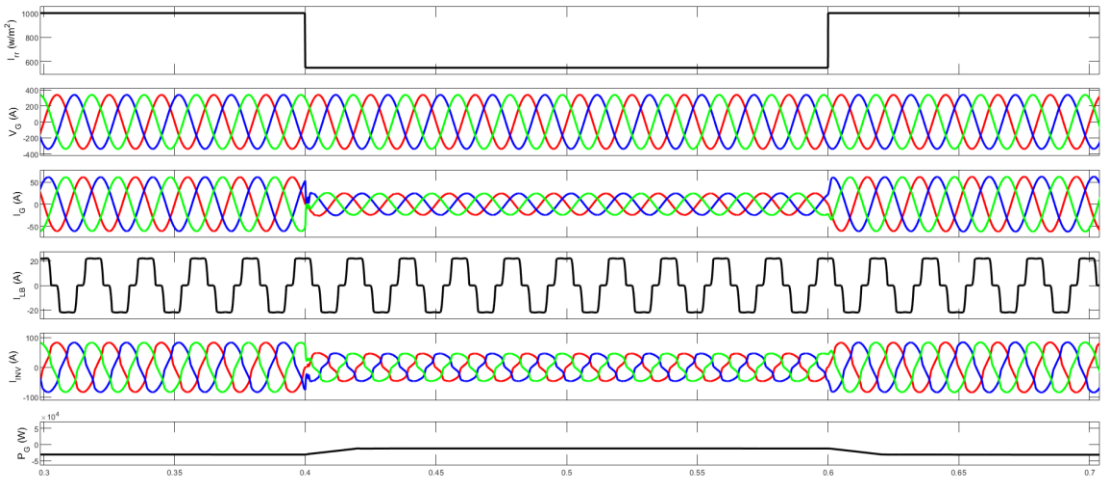

(a)

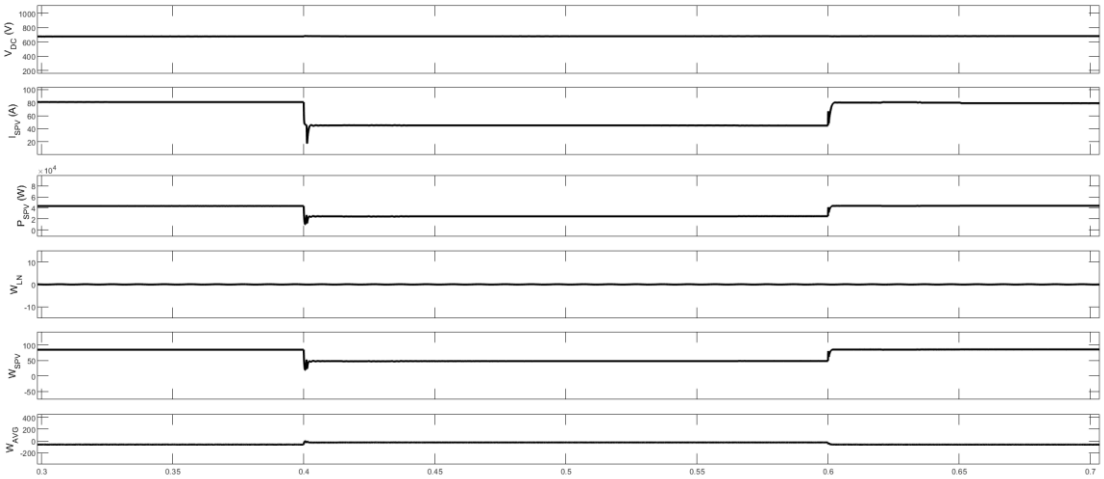

(b)

Fig. 5.14 (a) Shows the behavior of Solar irradiance (Irr), Grid voltage (VG), Grid current (IG), Inverter current (I_{inv}) and Grid power (P_G). (b) shows the characteristics of VDC, I_{SPV}, $P_{SPV,}$ Weight component of load (W_{LN}), PV weight Component (W_{SPV}) and Average weight (W_{AVG}).

5.4 Comparison of a Proposed MVZA-LMS against different LMS Model

Figure 5.15 illustrates the performance comparison of the mean-weight component of the load current (W_{LN}) under identical simulink environment. Performance of the

proposed Modified Versoria based Zero-Attraction algorithm in comparison with LMS, ZA-LMS and RZA-LMS is efficient, which has improved settling time and reduced steady state oscillation when subjected to dynamic situations. Table 5.1 shows the FFT analysis of different algorithm, and their THD values.

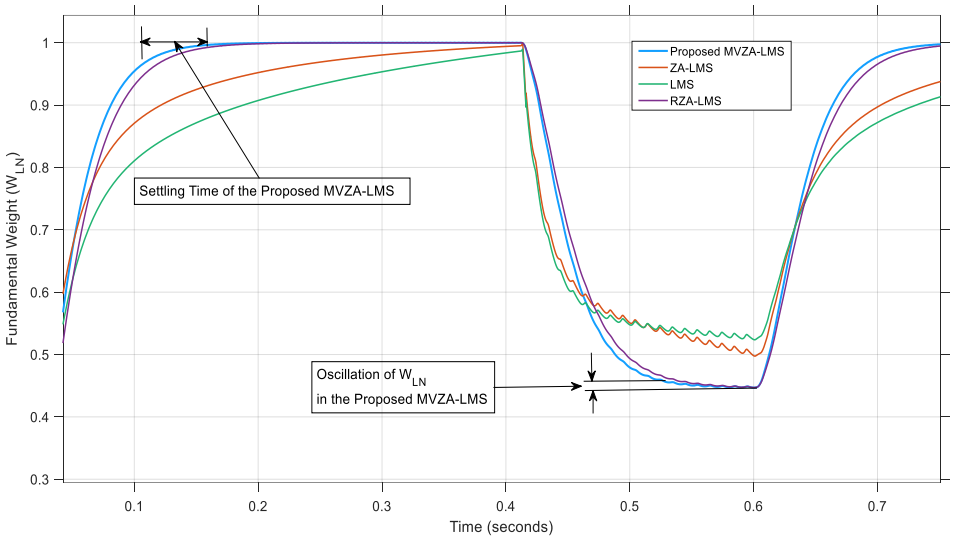

Fig 5.15 Performance comparison of proposed algorithm with other control Methodologies.

Table 5.1 THD comparison of different Algorithm with the proposed MVZA-LMS

Quantity	**LMS**	**ZA-LMS**	**RZA-LMS**	**MVZA-LMS**
% THD	1.58	1.18	1.12	1.06
I_G Magnitude	75.3	75.39	75.47	76.54
% THD	0.04	0.03	0.04	0.04
V_G Magnitude	338.8	338.8	338.8	338.8
% THD	23.63	23.63	23.63	23.63
I_{LB} Magnitude	23.93	23.93	23.93	23.93
% THD	6.60	6.60	6.60	6.60
I_{inv} Magnitude	93.89	93.89	93.94	98.89

CHAPTER 6

CONCLUSION

Simulink, coupled with MATLAB, serves as a modelling tool for the two-level conversion of power architecture in grid-connected SPGS (Solar Photovoltaic Generation Systems). The primary objective of the suggested control mechanism is to achieve load balancing, maintain operation at Unity Power Factor (UPF), and mitigate harmonics to enhance power quality at the Point of Common Coupling (PCC). This proposed research provides valuable insights into control schemes.

To regulate the Voltage Source Converter (VSC), an indirect current control approach is utilized to generate the necessary switching pulses. The suggested approach, known as MVZA-LMS (Modified Versoria Zero Attraction-Least Mean Square), evaluates the active component of the load current. The Proportional-Integral (PI) control method is employed to determine the weight factor of the DC-link. Comparative analysis with other control methodologies, including ZA-LMS, RZA-LMS, LMS reveals that the suggested MVZA-LMS control technique significantly reduces the Total Harmonic Distortion (THD) of the grid current. Upon evaluating the outputs, it can be concluded that the performance of the proposed model surpasses that of many zero-attractor based LMS controllers.

The proposed algorithm exhibits a fast convergence rate and robustness, while also reducing computational complexity. Moreover, the THD achieved aligns with the standards set by IEEE-519.

FUTURE SCOPE

In the future, further research can be conducted to explore additional control strategies and algorithms for power conversion in grid-interconnected SPGS. This could involve investigating advanced control techniques such as predictive control, fuzzy logic control, or neural network-based control. Additionally, the integration of energy storage systems, such as batteries or supercapacitors, can be explored to enhance the stability and reliability of the grid-connected SPGS. The application of advanced optimization algorithms to improve the efficiency and performance of the power conversion system is also a promising area for future investigation. Furthermore, the scalability and applicability of the proposed control mechanism can be explored for larger-scale renewable energy systems and microgrids.

PUBLICATIONS

[1] M. Akhlaque, J. Rai, S. Nagarajan, " Modified Versoria Function-Based Fast Zero Attraction LMS Algorithm applied to Grid Tied Solar PV System," presented in, Recent Advances in Electrical, Electronics and Digital Healthcare Technologies-2023 (REEDCON 2023), New Delhi, India, on 1st May, 2023.

REFERENCES

[1] Gielen, D., Boshell, F., Saygin, D., Bazilian, M. D., Wagner, N., & Gorini, R. (2019). The role of renewable energy in the global energy transformation. Energy Strategy Reviews, 24, 38-5

[2] M.G. Villalva, J.R. Gazoli, and E. Ruppert Filho, "Comprehensive approach to modeling and simulation of photovoltaic arrays," IEEE Trans. Power Electron., vol. 24, no.5, pp.1198-1208, May 2009.

[3] N. Pandiarajan and R. Muthu, "Viability analysis on photovoltaic configurations," in Proceedings of the IEEE Region 10 Conference (TENCON '08), Hyderabad, India, November 2008.

[4] J. A. Gow and C. D. Manning, "Development of a photovoltaic array model for use in power-electronics simulation studies," IEE Proceedings on Electric Power Applications, vol. 146, no. 2, pp. 193–200, 1999.

[5] M. Veerachary, "PSIM circuit-oriented simulator model for the nonlinear photovoltaic sources," IEEE Transactions on Aerospace and Electronic Systems, vol. 42, no. 2, pp. 735–740, 2006.

[6] "PV Balance of Systems Conference Berlin, Germany," June 2011.

[7] M. E. Ropp and S. Gonzalez, "Development of a MATLAB/simulink model of a single-phase grid-connected photovoltaic system," IEEE Transactions on Energy Conversion, vol. 24, no. 1, pp. 195–202, 2009.

[8] M. G. Villalva, J. R. Gazoli, and E. Ruppert Filho, "Modeling and circuit-based simulation of photovoltaic arrays," in Proceedings of the Brazilian Power Electronics Conference (COBEP '09), pp. 1244–1254, Bonito-Mato Grosso do Sul, Brazil, October 2009.

[9] S. Chowdhury, S. P. Chowdhury, G. A. Taylor, and Y. H. Song, "Mathematical modelling and performance evaluation of a stand-alone polycrystalline PV plant with MPPT facility," in Proceedings of the IEEE Power and Energy Society, General Meeting: Conversion and Delivery of Electrical Energy in the 21st Century (PES '08), Pittsburgh, Pa, USA, July 2008.

[10] B. H. Khan, Non-Conventional Energy Resources, McGraw Hill Education India Private Limited., 3rd Edition-2017.

[11] Aeronautics and Space Administration, (NASA-CR-149364) National, Solar Cell Array Design Handbook, vol. 1, Jet Propulsion Lab, 1976.

[12] M. Yamaguchi and A. Luque, "High efficiency and high concentration in photovoltaics," in IEEE Transactions on Electron Devices, vol. 46, no. 10, pp. 2139-2144, Oct. 1999.

[13] R. Har-Lavan and D. Cahen, "40 Years of Inversion Layer Solar Cells: From MOS to Conducting Polymer/Inorganic Hybrids," in IEEE Journal of Photovoltaics, vol. 3, no. 4, pp. 1443-1459, Oct. 2013.

[14] Y. Chen et al., "From Laboratory to Production: Learning Models of Efficiency and Manufacturing Cost of Industrial Crystalline Silicon and Thin-Film Photovoltaic Technologies," in IEEE Journal of Photovoltaics, vol. 8, no. 6, pp. 1531-1538, Nov. 2018.

[15] M. Gloeckler, I. Sankin and Z. Zhao, "CdTe Solar Cells at the Threshold to 20% Efficiency," in IEEE Journal of Photovoltaics, vol. 3, no. 4, pp. 1389-1393.

[16] Habbati Bellia, Ramdani Youcef, Moulay Fatima, A detailed modeling of photovoltaic module using MATLAB, NRIAG Journal of Astronomy and Geophysics, Volume 3, no. 1 pp, 53-61, 2014.

[17] A. V. Pavan Kumar, A. M. Parimi and K. Uma Rao, "Performance Analysis of a Two-Diode model of PV cell for PV based generation in MATLAB," 2014 IEEE International Conference on Advanced Communications, Control and Computing Technologies, Ramanathapuram, India, 2014, pp. 68-72.

[18] Elgendy, M.A., Zahawy, B., Atkinson, D.J.: Assessment of perturb and observe MPPT algorithm implementation techniques for PV pumping application. IEEE Trans. Sustainable Energy 3, 21– 33 (2012).

[19] Chou, Yang, and Chen, “Maximum Power Point Tracking of Photovoltaic System Based on Reinforcement Learning,” Sensors, vol. 19, no. 22, p. 5054, Nov. 2019.

[20] . Fangrui Liu, Yong Kang, Yu Zhang and Shanxu Duan, “Comparison of P&O and hill Climbing MPPT methods for grid-connected PV converter,” 3rd IEEE Conference on Industrial Electronics and Applications, 2008. ICIEA 2008, August 2008, pp. 804 – 807.

[21] 11Liu, F., Duan, S., Liu, F., Liu, B., Kang, Y.: A variable step size INC MPPT method for PV systems. IEEE Trans. Ind. Electron. 81(7), 2622– 2628 (2008).

[22] Elgendy, M.A., Zahawy, B., Atkinson, D.J.: Assessment of the incremental conductance maximum power point tracking algorithm. IEEE Trans. Sustainable Energy 4(1), 108– 117 (2013).

[23] Pathak, P.K., Yadav, A.K.: Design of battery charging circuit through intelligent MPPT using SPV system. Sol. Energy 178, 79– 89 (2019).

[24] Esram, T. and Chapman, P.L., “Comparison of Photovoltaic array maximum power point tracking techniques,” IEEE Transactions on Energy Conversion, vol.22, May 2007, pp.439 - 449.

[25] Lasheen, M., Abdel-Salam, M.: Maximum power point tracking using hill climbing and ANFIS techniques for PV applications: A review and a novel hybrid approach. Energy Convers. Manage. 171, 1002– 1019 (2018).

[26] A. Stephen, K. Musasa, and I. E. Davidson, “Modelling of Solar PV under Varying Condition with an Improved Incremental Conductance and Integral Regulator,” Energies, vol. 15, no. 7, p. 2405, Mar. 2022.

[27] Pathak, Pawan & Padmanaban, Sanjeevikumar & Yadav, Anil & Alvi, Dr. Parvez & Khan, Baseem. (2022). Modified incremental conductance MPPT algorithm for SPV based grid-tied and stand-alone systems. IET Generation, Transmission and Distribution.

[28] Aouchiche, N.; Cheikh, M.A.; Becherif, M.; Ebrahim, M.A.; Hadjarab, A. Fuzzy Logic Approach Based MPPT for the Dynamic Performance Improvement for PV Systems. In Proceedings of the Fuzzy Logic Approach Based MPPT for the Dynamic Performance Improvement for PV Systems, Boumerdes, Algeria, 29–31 October 2017.

[29] Mohammad Haziq Ibrahim, Swee Peng Ang, Muhammad Norfauzi Dani, Mohammad Ishlah Rahman, Rafidah Petra, Sheik Mohammed Sulthan, "Optimizing Step-Size of Perturb & Observe and Incremental Conductance MPPT Techniques Using PSO for Grid-Tied PV System", IEEE Access, vol.11, pp.13079-13090, 2023.

[30] Pavlos S. Georgilakis, Nikos D. Hatziargyriou, A review of power distribution planning in the modern power systems era: Models, methods and future research, Electric Power Systems Research, Volume 121, 2015.

[31] C. Sankaran, Power Quality, CRC Press, 2017.

[32] M.H.J. Bollen, What is power quality?, Electric Power Systems Research, Volume 66, Issue 1, Pages 5-14, 2003.

[33] . B. N. Alajmi et al., "A Multiport DC-DC Converter Based on Two-Quadrant Inverter Topology for PV Systems," IEEE Trans. on Power Electro., vol. 36, no. 1, pp. 522-532, Jan. 2021.

[34] Daniel Hart, Power Electronics, McGraw Hill Higher Education-2010.

[35] B. Singh, P. Jayaprakash, D. P. Kothari, A. Chandra, and K. Al Haddad, “Comprehensive study of DSTATCOM configurations,” IEEE Trans. Ind. Inform., vol. 10, no. 2, pp. 854-870, May 2014.

[36] C. Kumar and M. K. Mishra, “A multifunctional DSTATCOM operating under stiff source,” IEEE Trans. Ind. Elect., vol. 61, no. 7, pp. 3131-3136, July 2014.

[37] C. Kumar and M. K. Mishra, “An improved hybrid DSTATCOM topology to compensate reactive and nonlinear loads,” IEEE Trans. Ind. Elect., vol. 61, no. 12, pp. 6517-6527, Dec. 2014.

[38] B. Singh, A. Chandra, and K. Al-Haddad, Power Quality: Problems and Mitigation Techniques. Hoboken, NJ, USA: Wiley, 2015.

[39] Bhim Singh, K. Al-Haddad and A. Chandra, "A review of active filters for power quality improvement," IEEE Trans. Industrial Electronics, vol.46, no.5, pp.960-971, Oct 1999.

[40] M. Badoni, A. Singh and B. Singh, “Comparative performance of wiener filter and adaptive least mean square-based control for power quality improvement,” IEEE Trans. Ind. Elect., vol. 63, no. 5, pp. 3028-3037, May 2016.

[41] V. N. Kumar et al., "Improved Power Quality in a Solar PV PlantIntegrated Utility Grid by Employing a Novel Adaptive CurrentRegulator," IEEE Sys. Journal, vol. 14, no. 3, pp. 4308-4319, Sept.2020.

[42] S. K. Sahoo et al., "VSSMLMS-based control of multifunctional PVDSTATCOM system in the distribution network," IET Gener.,Transmis. & Distribt., vol. 14, no. 11, pp. 2100-2110, 2020.

[43] S. Haykin, Adaptive Filter Theory, 4th ed., Pearson Education, New Delhi, India, 2005.

[44] J. Chen, C. Richard, Y. Song, and D. Brie, "Transient performanceanalysis of zero-attracting LMS," IEEE Signal Process. Lett., vol. 23, no. 12, pp. 1786-1790, Dec. 2016.

[45] S. A. Rana, M. Jamil, M. A. Khan and M. N. Aalam, "Zero Attracting Mixed Norm LMS (ZA-MNLMS) Control for Two-Stage Power Conversion of Grid Interfaced Solar PV System," 2022 IEEE Delhi Section Conference (DELCON), New Delhi, India, 2022, pp. 1-5.

[46] Badoni, M., Singh, A., Singh, V. P., & Tripathi, R. N. (2018). Grid interfaced solar photovoltaic system using ZA-LMS based control algorithm. Electric Power Systems Research, 160, 261–272.

[47] S. S. Bhattacharjee, D. Ray and N. V. George, "Adaptive Modified Versoria Zero Attraction Least Mean Square Algorithms," in IEEE Transactions on Circuits and Systems II: Express Briefs, vol. 67, no. 12, pp. 3602-3606, Dec. 2020.

[48] M. Elad, Sparse and redundant representations: from theory to applications in signal and image processing. Springer Science & Business Media, 2010.

[49] F. Huang, J. Zhang, and S. Zhang, "Maximum Versoria Criterion-based Robust Adaptive Filtering Algorithm," IEEE Transactions on Circuits and Systems II: Express Briefs, vol. 64, no. 10, pp. 1252–1256, 2017.

[50] D. Ray, N. V. George, and P. K. Meher, "Analysis and design of unified architectures for zero-attraction-based sparse adaptive filters," IEEE Transactions on Very Large Scale Integration (VLSI) Systems, vol. 28, no. 5, pp. 1321–1325, 2020.

[51] G. Gui, W. Peng and F. Adachi, "Adaptive system identification using robust LMS/F algorithm", Int. J. Comm. Systems, pp. 2956–2963, 2014.

[52] Shahzad Ali Rana, Majid Jamil, Mumtaz Ahmad Khan, "A Robust Adaptive Inverse Hyperbolic Sine Function (RA-IHSF)-based Controlled Solar PV Grid Integrated System", Arabian Journal for Science and Engineering, 2023.

[53] IEEE Recommended Practices and requirement for Harmonic Control on Electric Power System, IEEE Std.519, 1992.

[54] M. H. Rashid, Power electronics handbook: Butterworth-Heinemann, (2017).

[55] A. Yazdani and R. Iravani, Voltage-sourced converters in power systems: modeling, control, and applications: John Wiley & Sons, (2010).

[56] Sivashanmugam, R., & Arumugam, S. (2016). Robust Adaptive Algorithm by an Adaptive Zero Attractor Controller of ZA-LMS Algorithm. Mathematical Problems in Engineering, 2016, 1–7.

[57] S. R. Arya, B. Singh, R. Niwas, A. Chandra and K. Al-Haddad, "Power Quality Enhancement Using DSTATCOM in Distributed Power Generation System," in IEEE Transactions on Industry Applications, vol. 52, no. 6, pp. 5203-5212, Nov.-Dec. 2016.

[58] https://powermin.gov.in/en/content/overview